

# White paper on ( $\alpha, n$ ) neutron yield calculations

D. Cano-Ott,<sup>1</sup> S. Cebrián,<sup>2</sup> M. Gromov,<sup>3,4</sup> M. Harańczyk,<sup>5</sup> A. Kish,<sup>6</sup> H. Kluck,<sup>7</sup> V. A. Kudryavtsev,<sup>8</sup> I. Lazanu,<sup>9</sup> V. Lozza,<sup>10,11</sup> G. Luzón,<sup>2</sup> E. Mendoza,<sup>1</sup> M. Parvu,<sup>9</sup> V. Pesudo,<sup>1</sup> A. Pocar,<sup>12</sup> R. Santorelli,<sup>1, a</sup> M. Selvi,<sup>13</sup> S. Westerdale,<sup>14</sup> and G. Zuzel<sup>5</sup>

<sup>1</sup>CIEMAT, Centro de Investigaciones Energéticas,  
Medioambientales y Tecnológicas, Madrid 28040, Spain

<sup>2</sup>CAPA, Centro de Astropartículas y Física de Altas Energías,  
Universidad de Zaragoza, Zaragoza 50009, Spain

<sup>3</sup>Skobeltsyn Institute of Nuclear Physics, Lomonosov Moscow State University, Moscow 119234, Russia

<sup>4</sup>Joint Institute for Nuclear Research, Dubna 141980, Russia

<sup>5</sup>M. Smoluchowski Institute of Physics, Jagiellonian University, 30-348 Krakow, Poland

<sup>6</sup>Fermi National Accelerator Laboratory, Batavia, IL 60510, U.S.A

<sup>7</sup>Institut für Hochenergiephysik der Österreichischen Akademie der Wissenschaften, 1050 Wien, Austria

<sup>8</sup>Department of Physics and Astronomy, University of Sheffield, Sheffield S3 7RH, UK

<sup>9</sup>Faculty of Physics, University of Bucharest, POBox 11, 077125, Magurele, Romania

<sup>10</sup>Laboratório de Instrumentação e Física Experimental de Partículas (LIP), 1649-003, Lisboa, Portugal

<sup>11</sup>Universidade de Lisboa, Faculdade de Ciências (FCUL),  
Departamento de Física, 1749-016 Lisboa, Portugal

<sup>12</sup>Amherst Center for Fundamental Interactions and Physics Department,  
University of Massachusetts, Amherst, MA 01003, USA

<sup>13</sup>INFN - Sezione di Bologna, Bologna 40126, Italy

<sup>14</sup>Department of Physics and Astronomy, University of California, Riverside, CA 92507, USA

(Dated: Tuesday 28<sup>th</sup> May, 2024- 02:41, Version: F1.0)

Understanding the radiogenic neutron production rate through the ( $\alpha, n$ ) reaction is essential in many fields of physics like dark matter searches, neutrino studies, nuclear astrophysics and medical physics. This white paper provides a review of the current landscape of ( $\alpha, n$ ) yields, neutron spectra and correlated  $\gamma$ -rays calculations, and describes the existing tools and the available cross sections. The uncertainties that contribute to ( $\alpha, n$ ) yield calculations are also discussed with plans for a program to improve the accuracy of these estimates. Novel ideas to measure ( $\alpha, n$ ) cross sections for a variety of materials of interest are presented. The goal of this study is to reduce the uncertainty in the expected sensitivity of next-generation physics experiments in the keV–MeV regime.

## CONTENTS

### I. Introduction

3

---

<sup>a</sup> [alphan@ciemat.es](mailto:alphan@ciemat.es)

	2
II. Process Description	4
III. Importance of ( $\alpha$ , n) reactions in different fields and relevant isotopes	5
A. Searches for rare events	5
1. ( $\alpha$ , n) induced backgrounds	5
2. Material screening techniques to suppress alpha emission	6
B. Nuclear astrophysics	9
C. Neutron sources	10
D. Nuclear technologies	11
E. Medical applications	11
IV. Measured and calculated ( $\alpha$ , n) cross-sections	13
A. Databases	15
B. Models	17
V. Neutron yield calculation tools	18
A. Stopping power calculation	19
B. SOURCES4	20
C. NeuCBOT	21
D. SaG4n	21
E. Comparison between the codes	22
VI. Typical uncertainties in neutron yield calculations	23
A. Cross sections: experimental data and nuclear model parameters	24
B. Assay results	30
C. Material composition	31
VII. Data needs	32
Acknowledgments	33
References	33

## I. INTRODUCTION

In recent years, a detailed understanding of the  $(\alpha, n)$  reaction has become increasingly important in various fields of physics <sup>1</sup>.

Neutrons are highly penetrating and can produce background signals that are indistinguishable from those expected from dark matter interactions in experiments such as DarkSide [1], CRESST [2], LZ [3], and XENON [4]. The  $(\alpha, n)$  reaction typically contributes significantly to the radiogenic backgrounds, therefore, obtaining accurate estimates of  $(\alpha, n)$  neutron production rates, energy spectra, and correlated  $\gamma$ -rays from the materials used in these detectors is essential.

Neutron fluxes are computed based on the results of material assays using codes that combine stopping power calculations with  $(\alpha, n)$  cross-sections, obtained from either measurements and/or theoretical models. However, the accuracy of radiogenic neutron background predictions in large detectors is limited by the significant uncertainties in  $(\alpha, n)$  yields [5–7]. For many isotopes and materials relevant to rare event search experiments, the uncertainty in  $(\alpha, n)$  yield is typically within 30 %, but it can be as high as  $\mathcal{O}(100\%)$ . The main sources of uncertainty are missing cross-section measurements, particularly for branching ratios to excited final states, or the theoretical models used to evaluate the  $(\alpha, n)$  reactions. In some cases, even when several sets of cross-section data are available for a specific material, discrepancies between experimental results have been observed, possibly due to differences in the experimental setups or the corrections applied when interpreting the results of the experiments. Furthermore,  $(\alpha, n)$  correlated  $\gamma$ -ray emission,  $(n, \gamma)$  cross-sections, and some decay data are also relevant for understanding detector triggers and vetoes for all rare event search experiments. For these applications, the energy region of interest extends up to 10 MeV, covering the range of  $\alpha$ -particle energies produced in <sup>235</sup>U, <sup>238</sup>U and <sup>232</sup>Th decay chains.

In addition, the knowledge of the neutron yield is vital in low-energy physics for neutrino experiments like DUNE [8], where  $(\alpha, n)$  neutrons produced by material contamination can be a potential source of background for supernova and solar neutrino studies. In particular,  $\gamma$ -rays emitted in neutron capture reactions can create signals up to 10 MeV, creating backgrounds for neutrino-electron scattering and for neutrino-nucleus interactions such as neutrino absorption. In nEXO [9], neutron can be captured on <sup>136</sup>Xe to form <sup>137</sup>Xe which, in turn, beta decays with a  $Q$ -value above the  $0\nu\beta\beta$  energy, creating background events in the ROI. The  $(\alpha, n)$  reactions can also create a background for JUNO [10] and SNO+ [11] searches, since the combination of the prompt neutron signal with the delayed capture can mimic the inverse beta decay of antineutrinos on protons. Additionally, high-energy gammas can fall in the energy region of interest for the nucleon decay and neutrino-less double-beta decay search.

Understanding the  $(\alpha, n)$  yields is also crucial for nuclear physics, nuclear astrophysics, and some nuclear energy related applications. For instance, they play an essential role in the sources of neutrons for the slow neutron capture processes, in radionuclide production by energetic solar particles, in the production of positron emitters, in the nucleosynthesis of light r-process nuclei in neutrino-driven winds, and in the production of neutrons by alpha emitters present in high-level nuclear waste.

Overall, there is a growing recognition of in-depth knowledge concerning the  $(\alpha, n)$  reaction.

---

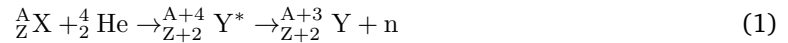
<sup>1</sup>This White Paper originated from the first workshop “ $(\alpha, n)$  yield in low background experiments,” which took place in Madrid in November 2019. Materials and conclusions from the meeting are available at this link: <https://agenda.ciemat.es/e/wan>.

The demand for greater sensitivity of the latest generations of rare-event search experiments and in nuclear astrophysics spurred an interest in improving the accuracy of  $(\alpha, n)$  yield calculations, as well as in evaluating the uncertainty in neutron production. In addition, novel techniques for measuring  $(\alpha, n)$  cross-sections for a variety of materials are being developed. As such, efforts to improve the accuracy of  $(\alpha, n)$  yield calculations and develop new techniques for measuring  $(\alpha, n)$  cross-sections will be an important area of research in the coming years.

This white paper aims to systematically discuss the most relevant aspects of calculating the  $(\alpha, n)$  neutron yield in low-background experiments. It compares the existing  $(\alpha, n)$  reaction codes and defines a common approach to uncertainties with a consistent treatment of model parameters. Moreover, it presents and discusses proposals to create a common repository of cross-sections that allows their use by different codes. The plans for measuring  $(\alpha, n)$  reactions relevant for underground experiments will also be presented and discussed.

## II. PROCESS DESCRIPTION

At the relatively low energy radiogenic regime ( $<10$  MeV), the  $(\alpha, n)$  reaction can be described as a two-step process:



In the first step, the capture of the  $\alpha$  by the target nucleus  $X$  populates an excited state of the compound  $X + \alpha \rightarrow Y^*$  nucleus. In a classical approach, the energy has to be enough to overcome the Coulomb repulsion of the two nuclei. Even though tunneling allows for the production of classically forbidden compound nuclei for a certain available energy, this is an important parameter percolating in the cross-section for this reaction. As a consequence, the nuclei expected to contribute more to neutron production are those with low- $Z$ , given the small Coulomb barrier. This notwithstanding, some mid- $Z$  metals might have sizable contributions due to specific nuclear properties [12].

The second step of the  $(\alpha, n)$  reaction is where complexity can be introduced. In the simplest scenario, the neutron drips off the compound nucleus  ${}^{A+4}Y$ . This is allowed when the populated  ${}^{A+4}Y^*$  state is above a certain threshold (denoted as  $S_n$ ). Assuming this scenario in which no other particles are involved and the decay goes to the ground state of  ${}^{A+3}Y$ , the energy of the neutron is

$$E_n = \frac{A+3}{A+4} [E(Y^*) + (M({}^{A+4}Y) - M({}^{A+3}Y))c^2], \quad (2)$$

and, since all the states above  $S_n$  are in the continuum,  $E$  can have any value above

$$E_n = \frac{A+3}{A+4} [S_n + (M({}^{A+4}Y) - M({}^{A+3}Y))c^2]. \quad (3)$$

Then, complexity can be added in many ways: the state of  ${}^{A+3}Y$  following neutron emission might not be the ground state, making it an  $(\alpha, n\gamma)$  reaction or a  $(\alpha, 2n)$  if such state is above

$S_n(A+3Y)$ ; if  $E(A+4Y) > S_{2n}(A+4Y)$  two neutrons can drip off simultaneously from the compound nucleus; states above  $S_p$  would induce proton decays. How this complex behaviour is commonly modeled in a statistical approach is summarized in Section IV B and the related uncertainties are discussed in Section VI A.

The detection of neutron-gamma coincidences and neutron emission with multiplicity 2 or larger is challenging. The mean free path of both gammas and neutrons is large compared with other types of ionizing radiation. This is especially true for neutrons, which generally suffer from low detection efficiency. Coincidences with neutrons are often characterized by extremely low detection efficiency. Detecting such final states with high resolution and statistics requires high coverage, high granularity detectors, and high-intensity beams (see for instance [13]). As a result, data for  $(\alpha, n\gamma)$  and  $(\alpha, Xn)$  cross-sections are particularly limited, and the term  $(\alpha, n)$  is often used neglecting this richness to refer to all the family of  $(\alpha, xn)$  processes, where  $x$  denotes anything emitted in addition to a single neutron (see Section IV for a discussion on the available data and calculations).

The overall contribution of these higher multiplicity channels is, however, subdominant. Where  $(\alpha, 2n)$  is most energetically favorable among the light elements are  $^{18}\text{O}$  (7.5 MeV),  $^{22}\text{Ne}$  (7.8 MeV) and  $^{26}\text{Mg}$  (8.4 MeV), which are barely accessible with radiogenic  $\alpha$  particles –this channel is only open for the 8.95 MeV  $\alpha$  decay of  $^{212}\text{Po}$  decay in the  $^{232}\text{Th}$  chain–, and higher multiplicity is even more disfavored.

### III. IMPORTANCE OF $(\alpha, n)$ REACTIONS IN DIFFERENT FIELDS AND RELEVANT ISOTOPES

#### A. Searches for rare events

Neutron radiation from  $(\alpha, n)$  reactions is a serious concern for rare event search experiments that require very low levels of radioactive background, such as the direct detection of dark matter or searches for neutrino-less double beta decay. If the detector's components or materials are contaminated with naturally occurring radioactive isotopes, e.g.  $^{235}\text{U}$ ,  $^{238}\text{U}$  and  $^{232}\text{Th}$ , their decay chains, which contain many  $\alpha$ -emitters, can produce a considerable neutron background that would limit experimental sensitivity. Thus, the material composition should always be carefully selected and used as an input to Monte Carlo simulations that are performed to evaluate potential backgrounds, as explained in Section V.

##### 1. $(\alpha, n)$ induced backgrounds

A material often used in low background experiments because of its high radio-purity is polytetrafluoroethylene (PTFE, or Teflon<sup>TM</sup>). PTFE also features good dielectric properties and high reflectivity for vacuum-ultraviolet (VUV) light. It is commonly used in cryogenic environment, e.g., for a variety of insulating structural elements, including cables supports. It is also used to reduce friction between metal parts, and as a reflector to enhance collection of light generated by plastic/liquid scintillators and noble elements, such as argon and xenon.

PTFE contains fluorine whose only stable isotope is  $^{19}\text{F}$ , which has a low threshold (around 2.3 MeV) for  $(\alpha, n)$  reaction and a steeply rising cross-section with energy. While several measure-

ments and model predictions of this cross-section exist, experimental data show a large spread and the resonance-like behavior is not properly described by these models. Other isotopes with  $(\alpha, n)$  cross-sections relevant for rare-event searches include:

- carbon ( $^{13}\text{C}$ ) contained in plastics, polyethylene, PTFE, scintillators and e.g. in rock surrounding underground experimental caverns,
- nitrogen ( $^{14}\text{N}$ ) present in some plastics and often used as inert buffer gas,
- oxygen ( $^{17}\text{O}$ ,  $^{18}\text{O}$ ) abundant in plastics, quartz, rock and water,
- silicon (predominantly  $^{29}\text{Si}$  and  $^{30}\text{Si}$ ) contained in various types of glass and quartz and used for widely used semiconductor detectors,
- aluminium ( $^{27}\text{Al}$ ), present in ceramics and sapphire,
- titanium, (stainless) steel, and copper (all naturally occurring isotopes), that are used to build cryostat vessels, support structures, and shielding,
- beryllium ( $^9\text{Be}$ ) present in wires and connection pins made out of CuBe alloy,
- sodium, chlorine, calcium and other elements found in rocks.

Considering natural radioactivity, beside the  $(\alpha, n)$  reactions, spontaneous fission also contributes to neutron production: Spontaneous fission (SF), as described by Watt's formulae [14], gives the same neutron yield for all materials and depends only on the concentration of the fissioning isotope. Among naturally occurring radioactive isotopes, only fission of  $^{238}\text{U}$  contributes significantly to neutron production. Although the probability of SF of  $^{238}\text{U}$  is about  $5 \times 10^{-7}$  compared to  $\alpha$  decay rate, the neutron yield from this process dominates over that from  $(\alpha, n)$  reactions for high- $Z$  materials where the neutron production is highly suppressed due to the Coulomb barrier. In practice, neutrons produced in the SF process can be tagged with high efficiency in a detector or a veto system due to simultaneous emission of several neutrons and  $\gamma$ -rays.

Neutron yield from  $(\alpha, n)$  reactions depends on the energy of alpha particles, the cross-section of the reaction, and the alpha energy loss in a particular material. The two most common natural radioactive decay chains,  $^{232}\text{Th}$  and  $^{238}\text{U}$ , are critical in the calculation of neutron background for low background experiments. They produce 6 and 8  $\alpha$  decays, respectively. The energies of each alpha in the decay chain need to be considered. The decay chain of  $^{235}\text{U}$ , which comprises 7  $\alpha$  decays, also contributes to neutron production, although generally less due to the small abundance of  $^{235}\text{U}$  in natural Uranium (0.72%). Finally, secular equilibrium in the decay chains is often broken, especially for  $^{238}\text{U}$ .

## 2. Material screening techniques to suppress alpha emission

For illustration, in Fig. 1 a simplified decay scheme of the  $^{238}\text{U}$  decay chain is shown. The black box includes the top part of the chain with the long-lived U/Th isotopes (3  $\alpha$ -decays). The red box indicates the middle part of the chain with  $^{226}\text{Ra}$ ,  $^{222}\text{Rn}$  and its short-lived daughters (4  $\alpha$ -decays). Finally, the bottom part of the chain is shown in the yellow box, including the so-called "long-lived  $^{222}\text{Rn}$  daughters" (one  $\alpha$ -decay). The secular equilibrium is usually broken at the level of  $^{226}\text{Ra}$  and  $^{210}\text{Pb}$ . Due to the relatively short half-lives of their daughters, we can assume that the respective sub-chains are in equilibrium. Because U/Th and Ra are different elements with

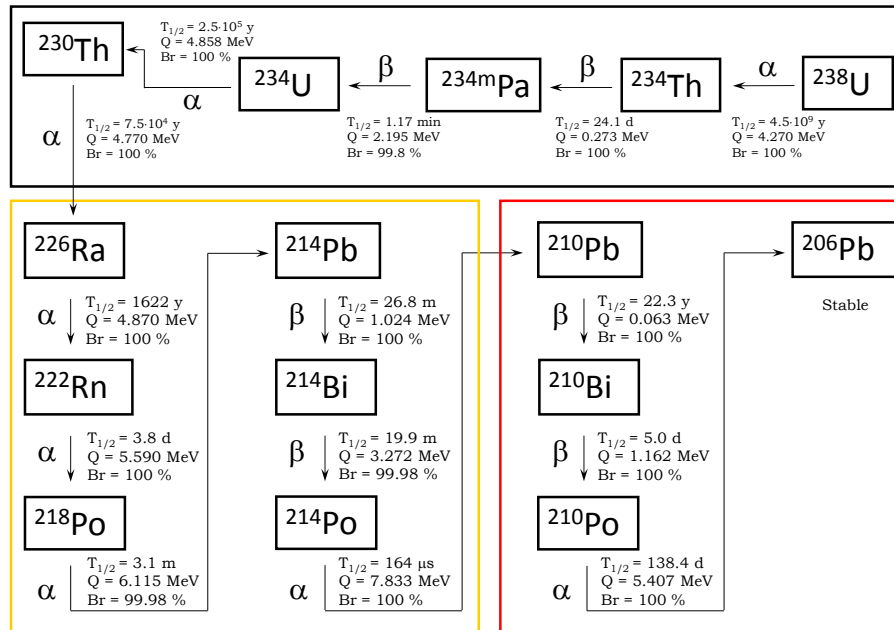


FIG. 1:  $^{238}\text{U}$  decay chain. The chain is divided into three parts, in which the long-lived U/Th isotopes (top),  $^{226}\text{Ra}$  with  $^{222}\text{Rn}$  and its short-lived daughters (bottom left), and the long-lived  $^{222}\text{Rn}$  daughters (bottom right) appear. The three parts are usually in disequilibrium thus, they should be assayed separately.

different chemical properties, materials which undergo production processes are usually enriched or depleted with Radium with respect to Uranium. Moreover, due to the 22 yr half-life of  $^{210}\text{Pb}$  there is usually disequilibrium between the short- and the long-lived  $^{222}\text{Rn}$  daughters. This is why it is not recommended to conclude about the specific activities of  $^{226}\text{Ra}$  (and  $^{222}\text{Rn}$ ) from e.g. the ICP-MS measurements (determination of U/Th). The same concerns the bottom part of the  $^{238}\text{U}$  chain: it is usually not possible to predict the activities of  $^{210}\text{Pb}$  –  $^{210}\text{Po}$  from the high-sensitivity  $^{222}\text{Rn}$  emanation measurements, or from the  $\gamma$ -ray screening. Therefore, in order to predict properly the background rates caused by a particular element of the detector, it is necessary to assay each part of the chain separately. Clearly, depending on the experiment and its goal, different sub-chains may contribute differently, but usually the most important is  $^{226}\text{Ra}/^{222}\text{Rn}$  and their long-lived decay products. Therefore, in the last years strong emphasis has been put on developments of high-sensitivity  $\gamma$ -ray spectrometers, Radon emanation techniques and alpha spectroscopy.

A disequilibrium effect has been observed for example for the nylon foil, which was used to construct the Borexino scintillator vessel [15]. In most of the investigated samples the  $^{226}\text{Ra}$  activity concentrations were higher compared to  $^{238}\text{U}$ , but the last one showed a different behavior: Radium content was a factor 20 lower compared to Uranium and the effect was related to a different production process of the foil.

The foundation of the experiments devoted to searches for rare events is an extensive radioassay programs. Its goal is to perform a selection of materials and components, which can be used for

construction of respective detectors. The selection is based on the content of radioactive isotopes, where the allowed concentrations are determined applying extensive Monte Carlo simulations. Determined residual radioactivity for various components can vary significantly from different suppliers and even from production batches. A great deal of radio-purity measurements are available for materials like copper, stainless steel, PTFE, polyethylene, and for electronics and readout components (see for instance results compiled at <http://radiopurity.org> and at [16–23]). An accurate estimate of ( $\alpha$ , n) neutron yields requires the knowledge of radioactivity in the material to normalize the MC simulations.

Different techniques are commonly used in material screening. Mass spectrometry, like Inductively Coupled Plasma Mass Spectrometry (ICP-MS) or Glow Discharge Mass Spectrometry (GDMS) are used to detect U and Th in samples. Thus, only the activity concentrations of isotopes in the upper part of the chains of  $^{238}\text{U}$  (upper box in Fig. 1) and  $^{232}\text{Th}$  can be deduced. However, mass spectrometers are usually very sensitive and allow to perform measurements down to a sub-ppt (parts per trillion,  $10^{-12}$  g/g) level [24].

The  $\gamma$ -ray counting is a powerful and sensitive method to look for radio-impurities, without destroying the sample. It allows investigating the middle part of the  $^{238}\text{U}$  (mainly  $^{226}\text{Ra}$  and its daughters - see the red box in Fig. 1) and  $^{232}\text{Th}$ , as well as to  $^{40}\text{K}$ ,  $^{60}\text{Co}$ ,  $^{137}\text{Cs}$  and other gamma emitters. Assay time depends on the required sensitivity and can be as long as a couple of months. Sample size is usually limited to a few tens of kilograms because of the effects of the self-shielding. There are many  $\gamma$ -counting facilities around the world, but the most sensitive instruments are operated at the INFN Laboratori Nazionali del Gran Sasso and at the Canfranc Underground Laboratory reaching sensitivities of  $10\ \mu\text{Bq kg}^{-1}$  [25, 26]. In some cases (e.g. thin foils)  $^{226}\text{Ra}$  may be investigated by application of high sensitivity  $^{222}\text{Rn}$  emanation techniques, reaching similar or even better sensitivities [27] compared to  $\gamma$ -ray spectrometry.

To assay  $^{210}\text{Pb}$  in the bottom part of the U-chain (yellow box in Fig. 1) chemical extraction of  $^{210}\text{Po}$  is applied. The advantage of this method is that usually only a small mass is needed (a few g) for analysis. High purity concentrated acids like HCl,  $\text{HNO}_3$ , HF,  $\text{H}_2\text{SO}_4$  are used to dissolve samples. They are always spiked with  $^{208}\text{Po}$  or  $^{209}\text{Po}$  for determination of the chemical yield (Po extraction efficiency). If organic matter is present, also  $\text{H}_2\text{O}_2$  is added. Next, the mixture is converted into 0.5 M HCl solution from which Po is auto-deposited on a silver disc. In some cases, separation of Po from the matrix on a dedicated column is necessary. Po's activity is measured with a low background alpha spectrometer, with the overall efficiency deduced from the spike signal. Sensitivities down to  $0.5\ \text{mBq kg}^{-1}$  for  $^{210}\text{Po}$  are achievable. As an example, it has been found that the  $^{210}\text{Po}$  concentrations in copper follows the chemical purity of the material and changes from  $10\ \text{mBq kg}^{-1}$  (oxygen-free copper) up to  $10\ \text{Bq kg}^{-1}$  (fire-refined copper). Values obtained for low radioactivity lead ( $\approx 2\ \text{Bq kg}^{-1}$ ) were consistent with  $^{210}\text{Pb}$  measured via beta spectroscopy [28]. Activity concentrations deduced for high-purity titanium were at the level of  $2\ \text{Bq kg}^{-1}$ . The results confirmed the first assays of  $^{210}\text{Po}$  bulk activities in metals performed with application of large surface low background alpha spectrometer [29].

Another class of background source is the surface contamination with naturally occurring alpha emitters (mostly the short- and long-lived daughters of  $^{222}\text{Rn}$ ). Exposure to environmental Radon during fabrication, assembly, and installation of low background systems can lead to build-up of  $^{210}\text{Pb}$  on surfaces being in contact with the active detector parts.  $^{210}\text{Pb}$  in the sub-surface layer can be accumulated though the diffusion of Radon.  $^{222}\text{Rn}$  atoms can penetrate layers up to several tens of  $\mu\text{m}$ , depending on the diffusion constant [30].  $^{210}\text{Pb}$  which has 22 yr half-life will therefore, act as an approximately constant source of radiation (from self decays and from decays of  $^{210}\text{Bi}$  and

$^{210}\text{Po}$ ) throughout the full life of an experiment. In case of surface contamination, the alpha decays are relatively easy to identify by their specific energies (e.g. 5.3 MeV for  $^{210}\text{Po}$ ). If the alpha peaks are shifted towards lower energies due to quenching effects (e.g. in the scintillators) the decays can still be recognized by application of the pulse shape analysis. Alpha decays occurring on the surfaces of materials that contain isotopes with high  $(\alpha, n)$  cross-sections (e.g. PTFE) will contribute significantly to the neutron background. Sensitive surface and bulk assay of  $^{210}\text{Po}$  may be carried out using low background large surface alpha spectrometers, like the XIA UltraLo-1800 [29]. Due to very low background and by analysis of the continuous part of the spectrum between 1.5 MeV and 6.0 MeV bulk  $^{210}\text{Po}$  may be assayed down to about  $50 \text{ mBq kg}^{-1}$  [15]. Looking at the peak around 5.3 MeV surface contamination, as low as  $0.5 \text{ mBq m}^{-2}$  may be determined [29]. To avoid problems related to surface contamination, it is recommended to store all detector components after production and before installation in a Radon-free atmosphere (in clean rooms supplied with Rn-free air or in multi-layer plastic bags that are impervious to Radon). Also, material-specific surface cleaning protocols should be applied.

Particular attention should also be paid to the final machining of structural materials. Modern detectors devoted to searches for rare processes are quite large and include tonnes of materials, such as metals or plastics. A small radiogenic contamination per unit mass/surface can lead to a significant  $(\alpha, n)$  background. Taking into account that the material is usually purchased not in the form of final products, but in the form of intermediate goods based on the results of the assays, extra amount of Uranium and Thorium may occasionally be introduced into structural components of the detector during the manufacturing and later machining processes. Therefore, the assays should be repeated after every stage of production, if possible. Ideally, such constant monitoring of radioactive contamination should be included in the technological chain of production of a structural element of the detector from the stage of purchasing raw materials to the stage of manufacturing the final product. Fortunately, there are several technologies that are already available and applied. This refers to the production of pure PMMA with/without gadolinium [31] and titanium [32, 33].

## B. Nuclear astrophysics

The nucleosynthesis, or creation of the elements in the Universe, is carried out via nuclear reactions [34, 35]. Charged particle reactions, especially those induced by the primary products of Big Bang nucleosynthesis (protons,  $^2\text{H}$ ,  $^3\text{He}$ , and  $\alpha$  particles) are the main process in the synthesis of the elements with  $A < 60$ . The overlap between the Coulomb barrier penetration probability and the temperature distribution of particle energies will determine the probability of these reactions to take place [36, 37].

The fundamental reaction in stars is the proton-proton fusion. After the hydrogen fuel is depleted, the star undergoes gravitational collapse reaching a higher temperature ( $\approx 10^8 \text{ K}$ ), thus the Coulomb barrier for  $^4\text{He}-^4\text{He}$  fusion can be overcome [36].

The  $(\alpha, n)$  reactions are crucial in various astrophysical mass ranges, providing insights into the origin of the elements. They are particularly important in the weak r-process (also called the  $\alpha$ -process), which occurs in the neutrino-driven ejecta of core-collapse supernovae and is responsible for producing lighter heavy elements observed in metal-poor stars. The uncertainty in their astrophysical rates is the primary factor affecting this process. In stars, the slow neutron-capture process (s-process) is one of the two main mechanisms responsible for the formation of elements heavier than iron. The efficiency of this process is heavily dependent on  $(\alpha, n)$  reactions, which serve as

the primary sources of neutrons that initiate the neutron-capture chain, resulting in the creation of elements up to Bismuth.

The  $^{22}\text{Ne}(\alpha, n)^{25}\text{Mg}$  and  $^{13}\text{C}(\alpha, n)^{16}\text{O}$  reactions are the main sources of neutrons for the s and i-processes (intermediate neutron capture process [38–40]), while  $(\alpha, n)$  reactions on  $17 < A < 34$  nuclei may impact nucleosynthesis in Type Ia supernova explosions. In the case of  $^{22}\text{Na}$ , the cross-section is mostly unknown in the relevant stellar energy range of 450–750 keV, where direct measurements provide only upper limits, and estimates from indirect sources are uncertain.  $^{13}\text{C}(\alpha, n)^{16}\text{O}$  reaction has been studied in [41–49] and experimental cross-sections exist in 0.3–8 MeV energy range.

In the low-mass regime, the  $^9\text{Be}(\alpha, n)^{12}\text{C}$  reaction is critical for both the s and r-processes, as well as for primordial nucleosynthesis.

For core-collapse supernovae explosions, particularly important reactions include  $^{96}\text{Zr}(\alpha, n)^{99}\text{Mo}$ ,  $^{100}\text{Mo}(\alpha, n)^{103}\text{Ru}$ ,  $^{86}\text{Kr}(\alpha, n)^{89}\text{Sr}$ .

The cross-sections of the  $^{96}\text{Zr}(\alpha, n)^{99}\text{Mo}$  and  $^{100}\text{Mo}(\alpha, n)^{103}\text{Ru}$  reactions were recently measured at energy ranges relevant to astrophysics [50, 51]. These measurements were conducted to better understand the parameters of the  $\alpha$ +nucleus optical potential.

Recently, the  $^{86}\text{Kr}(\alpha, n)^{89}\text{Sr}$  cross-section at an energy relevant for the weak r-process in the neutrino-driven winds of core-collapse supernovae has been measured in order to reduce uncertainty in model predictions for nucleosynthesis in this site [52].

### C. Neutron sources

The combination of an  $\alpha$  emitter and a low- $Z$  material is a typical method exploited to produce inexpensive and compact neutron sources, such as those used for calibration purposes in various types of experiments. Beryllium is a very common material used in  $\alpha$ -neutron sources, which can yield approximately  $10^{-4}$  neutrons per  $\alpha$ -decay through the reaction:



It is important to note that this particular process may also involve the emission of gamma radiation. Fluorine, lithium, carbon, and boron are other alternative materials with high  $\alpha$ -neutron cross-sections.

As for typical alpha emitters, the list includes  $^{241}\text{Am}$ ,  $^{238}\text{Pu}$ ,  $^{239}\text{Pu}$ ,  $^{210}\text{Po}$ , and  $^{226}\text{Ra}$  (see, for instance, [31]). The strength of the neutron source is determined by the activity of the  $\alpha$  emitter. Activities in the range of approximately 1–1000 GBq are common, although smaller or larger values are possible for special purposes. The actual neutron yield depends on the source matrix and, in particular, on the concentration of the  $\alpha$ -emitting isotope within the matrix.

The average (maximum) neutron energy of Am-Be and Pu-Be sources is  $\approx 4.2$  MeV (11 MeV). For Ra-Be source it is 3.6 MeV (13.2 MeV). Am-F and Am-Li sources have average neutron energies of 1.5 MeV and 0.5 MeV, respectively.

#### D. Nuclear technologies

Materials control and accountancy of uranium (U) and plutonium (Pu) throughout the fuel cycle heavily depend on a diverse range of passive and active neutron counting methods. Given that these materials are typically found in compound forms like oxides, fluorides, and carbides, with potential light element impurities such as lithium (Li), beryllium (Be), and boron (B), the production of neutrons via  $(\alpha, n)$  reactions often constitutes a notable source of neutron signals. Additionally, this phenomenon contributes significantly to self-interrogation in items undergoing multiplication [53].

Neutrons and  $\gamma$ -rays emitted during the  $(\alpha, n)$  process contribute to the total flux of radiation along the fuel cycle, from the enrichment and fuel fabrication, fuel reprocessing, and disposal of the spent fuel. More accurate data on the cross-sections, total neutron yields, neutron spectra, and  $\gamma$ -ray emissions from  $(\alpha, n)$  reactions are needed for reducing the (frequently large) uncertainties in neutron background and activation estimation, nuclear waste characterization, dosimetry, non-destructive mass assay of fresh and used nuclear fuel, nuclear safeguards, and materials control and accountancy. The thick target integrated over angle yield curve is perhaps the most important quantity for applications. However, thin-target data, neutron and  $\gamma$ -ray spectra are also needed, in particular data on partial cross-sections and angular distributions, for the calculation and evaluation of  $4\pi$  emission spectra.

$^{19}\text{F}(\alpha, n)$  and  $^{17,18}\text{O}(\alpha, n)$  can be considered as the most relevant reactions for fission reactor technologies. Other important nuclides in fission applications are lithium, beryllium, boron, carbon, nitrogen, sodium, aluminum, and silicon. The renewed interest in molten salt reactors may require new data on different salt components like lithium, beryllium, nitrogen, fluorine, sodium, and potassium. In addition, the development of fusion reactors requires improving  $(\alpha, n)$  data on structural materials and materials used for plasma diagnostics.

#### E. Medical applications

Most of the radiopharmaceuticals (95 %) are used in diagnostics as well as imaging techniques like SPECT or PET. These techniques can reveal the integrity and functions of organs, as well as metabolic pathways of radio-tracers in the body. Notwithstanding the economic aspects, to be efficient and safe to use, diagnostics radiopharmaceuticals should give a low dose of radiation, should be eliminated quickly from the body (having short effective half-lives) and should be trapped by the metabolic process of interest. Thus, a very specific and limited number of isotopes is considered. Radioisotopes used for these applications can be produced in nuclear reactors or through the irradiation of a target with particle accelerators using different particle beams. Thus,  $(\alpha, xn)$  reactions represent an important option.

Some of the radionuclides commonly produced using  $\alpha$ -particles are listed in Table I. [54].

For medical applications, the following types of isotopes are considered.

1. Radioactive isomeric states of a few nuclides have very suitable decay properties for therapeutic applications. In general, they are low-lying states with high nuclear spins. They decay mostly to their respective ground states by a high internal conversion transition. The low-energy conversion electrons, or an avalanche of emitted Auger electrons, can lead to precise localized internal therapy effects if the radioactive species is properly attached to an appro-

TABLE I: Radionuclides commonly produced using  $\alpha$ -particles.

Range of negative $Q$ -values / MeV	Residual isotope produced in the $(\alpha, n)$ reactions
[0,2]	$^{53}\text{Mn}$ , $^{51}\text{Ti}$ , $^{22}\text{Na}$
(2,4]	$^{54}\text{Mn}$ , $^{51}\text{Cr}$ , $^{48}\text{V}$ , $^{44}\text{Sc}$ , $^{43}\text{Sc}$ , $^{40}\text{K}$ , $^{36}\text{Ar}$ , $^{33}\text{S}$ , $^{30}\text{P}$ , $^{26}\text{Al}$
(4,6]	$^{53}\text{Fe}$ , $^{49}\text{Cr}$ , $^{45}\text{Ti}$ , $^{38}\text{K}$ , $^{37}\text{Ar}$ , $^{34}\text{Cl}$
(6,8]	$^{42}\text{Sc}$ , $^{27}\text{Si}$ , $^{23}\text{Mg}$
(8,10]	$^{47}\text{Cr}$ , $^{39}\text{Ca}$ , $^{35}\text{Ar}$ , $^{31}\text{S}$
> 10	$^{43}\text{Ti}$ , $^{21}\text{Mg}$

priate chemical carrier. Several such isomeric states can be mentioned:  $^{117m}\text{Sn}$ ,  $^{193m}\text{Pt}$  and  $^{195m}\text{Pt}$ , obtained in reactions  $(\alpha, xn)$ , with  $x = 1$  and 3 from  $^{116}\text{Cd}$  and  $^{192}\text{Os}$  [55].

2. Halogens are isotopes used for diagnosis and therapy in nuclear medicine. Fluorine ( $^{18}\text{F}$  with a half-life of 110 minutes) has the strongest carbon-halogen bond, but is limited to PET and has a too short half-life to study slow metabolic processes, i.e. of proteins and peptides [56]. Iodine on the other side has isotopes with different decay characteristics suitable for a broader spectrum of medical applications but the chemical bonding is sometimes too weak, and the labelled molecules are then not stable enough in vivo. Iodine isotopes are obtained as  $^{123}\text{Sb}(\alpha, xn)^{126,125,124}\text{I}$  reactions. Radionuclides from the bromine family are an alternative [57]. The positron emitters  $^{75}\text{Br}$  ( $T_{1/2} = 96.7$  min) and  $^{76}\text{Br}$  ( $T_{1/2} = 16.2$  h) could be used for medical applications. The  $^{77}\text{Br}$ , decaying by electron capture (half-life of 57 h) is a candidate in Auger-therapy, as well as the shorter-lived  $^{80m}\text{Br}$  ( $T_{1/2} = 4.4$  h), decaying by isomeric transition, while the  $\beta^-$ -emitter  $^{82}\text{Br}$  ( $T_{1/2} = 35.2$  h) is also a candidate for therapy applications. Alpha-particle induced reactions on arsenic  $^{75}\text{As}$  lead to  $^{76,77,78}\text{Br}$ .
3. A new option of cancer treatment is possible with the radioactive isotope ( $^{211}\text{At}$ ) [58, 59]. Results suggest that the short 7.2-hour half-life of radioactive isotope  $^{211}\text{At}$  can provide blood-borne cancer patients with just enough radiation therapy to target their cancer cells and minimizes exposure of the rest of the body; it also limits the exposure of the team that manipulated this radioisotope. The nuclear reaction that describes the production process of  $^{211}\text{At}$  in bismuth target is  $^{209}\text{Bi}(\alpha, 2n)^{211}\text{At}$  [60].
4. Isotopes  $^{43}\text{K}$  and  $^{30}\text{P}$  are also of interest for biological and medical studies. These isotopes can be produced by  $^{40}\text{Ar}(\alpha, p)^{43}\text{K}$  and  $^{30}\text{P}$  can be made from  $^{27}\text{Al}(\alpha, n)^{30}\text{P}$  [54]. Medically important isotopes are also  $^{110m}\text{In}$  and  $^{111}\text{In}$  [61]. Usually the isotope  $^{111}\text{In}$  is obtained in a cyclotron in the reaction  $^{112}\text{Cd}(p, 2n)^{111}\text{In}$  [62], but alternative reactions are possible:  $^{109}\text{Ag}(\alpha, 2n)$  for  $^{111}\text{In}$  and  $^{107}\text{Ag}(\alpha, n)$  or  $^{109}\text{Ag}(\alpha, 3n)$  for  $^{110m}\text{In}$ , respectively.

All the reactions using  $\alpha$ -particle beams have great advantages. The activation of materials in the beam of  $\alpha$ -particles, i.e. the formation of radioactive products, is an interesting topic of study both as fundamental research and for applications. The formation of nuclear isomeric states is difficult to reproduce by theory. The cross-section data obtained as a function of  $\alpha$ -particle energy are of great practical significance in the production of some medical-related radionuclides, although their yields are generally much lower than in proton or deuteron-induced reactions. There are several

radionuclides that are exclusively produced through the use of  $\alpha$ -particles, and there are a few low-lying high-spin isomeric states that are preferentially populated in  $\alpha$ -particle induced reactions.

#### IV. MEASURED AND CALCULATED ( $\alpha, n$ ) CROSS-SECTIONS

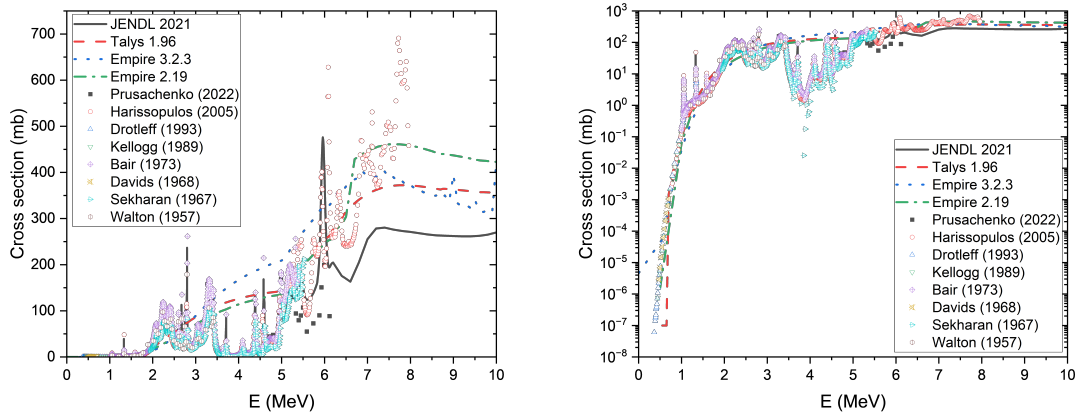


FIG. 2:  $^{13}\text{C}(\alpha, n)^{16}\text{O}$  cross-section as a function of energy.

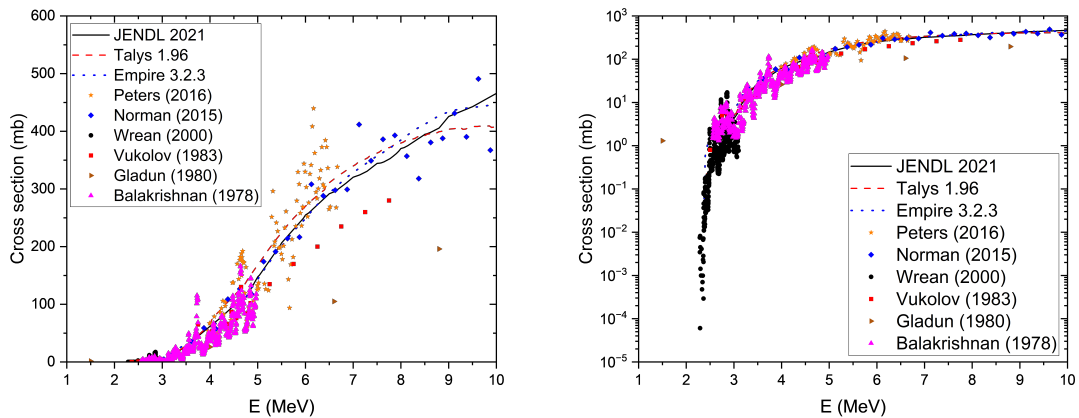


FIG. 3:  $^{19}\text{F}(\alpha, n)^{22}\text{Na}$  cross-section as a function of energy.

The energy-dependent cross-sections of ( $\alpha, n$ ) reactions are isotope-dependent and can be calcu-

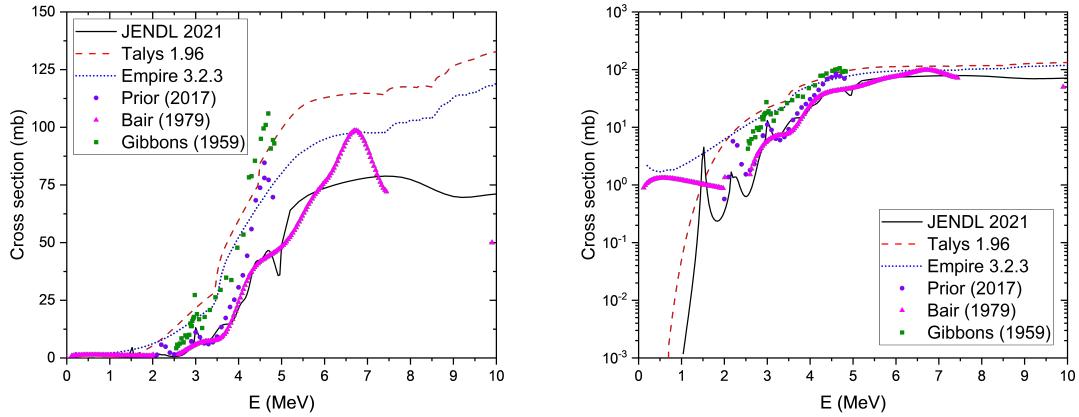


FIG. 4:  $^{10}\text{B}(\alpha, n)^{13}\text{N}$  cross-section as a function of energy.

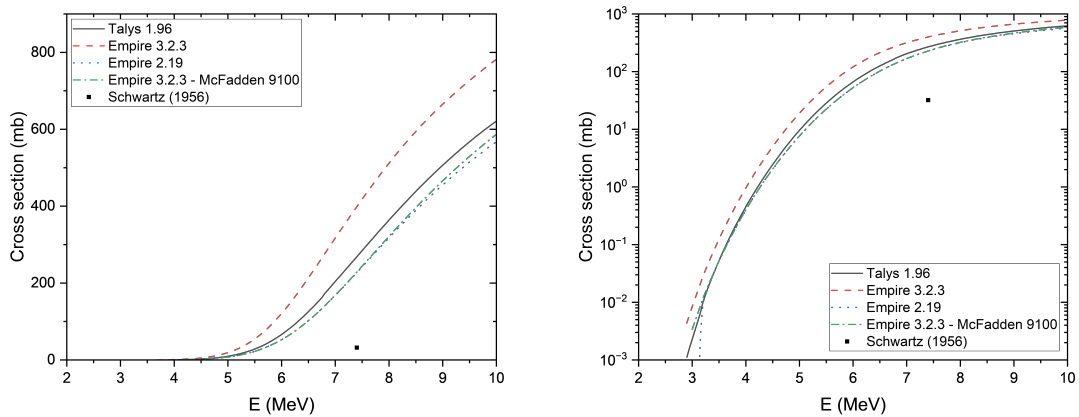


FIG. 5:  $^{40}\text{Ar}(\alpha, n)^{43}\text{Ca}$  cross-section as a function of energy.

lated using nuclear physics codes, such as `EMPIRE`<sup>2</sup> [63, 64] or `TALYS`<sup>3</sup> [65, 66], or taken directly from experimental data when available. They can also be taken from available libraries, either evaluated like `JENDL` [67] or produced using the toolkits as above, like `TENDL` [68] containing a library of cross-sections from the `TALYS` code. The energy threshold of these reactions is determined by the  $Q$ -value of the reaction and the Coulomb barrier that suppresses the reaction probability even if the  $\alpha$ -particle energy is above the threshold determined by the  $Q$ -value. Hence, the  $(\alpha, n)$  reac-

<sup>2</sup>Currently in version 3.2 available at <https://www-nds.iaea.org/empire/>.

<sup>3</sup>Currently in version 1.96 available at <https://www-nds.iaea.org/talys/>.

tions are important for low- and medium- $Z$  nuclei while the neutron yield per unit concentration of a radioactive isotope from elements heavier than copper is quite small. Figures 2 to 5 show a comparison of cross-section data taken from different sources for different target nuclei.

### A. Databases

The Experimental Nuclear Reaction Data (EXFOR) library [69] (CSISRS in USA) contains an extensive compilation of experimental nuclear reaction data, based on numerical data sets and bibliographical information of 22 000 experiments since the beginning of nuclear science and it is updated monthly. The associated online database retrieval system provides access to data (by selecting a target, reaction, quantity, or energy range) and different tools for plotting and data comparison. It is publicly available at the websites of the International Atomic Energy Agency Nuclear Data Section<sup>4</sup>, the U.S. National Nuclear Data Center<sup>5</sup> and several mirrors.

The availability of experimental cross-section across the entire energy spectrum of interest can be limited. Experimental data can be absent for some specific materials.

On the other hand, only two sets of evaluated ( $\alpha, n$ ) cross-section data libraries are available.

JENDL (Japanese Evaluated Nuclear Data Library) [67] provides a library of reaction data for various application fields (the so-called “general purpose files”) and a set of extra libraries for some particular application field (“special purpose files”)<sup>6</sup>. The latest release of the main library was in 2021, named JENDL-5. Among others, it includes information for 795 nuclides for neutron-induced reactions and 18 nuclides for alpha-induced reactions in the energy range up to 200 MeV and 15 MeV, respectively. These 18 nuclides are important mainly in nuclear fuel-cycle applications. They are <sup>6</sup>Li, <sup>7</sup>Li, <sup>9</sup>Be, <sup>10</sup>B, <sup>11</sup>B, <sup>12</sup>C, <sup>13</sup>C, <sup>14</sup>N, <sup>15</sup>N, <sup>17</sup>O, <sup>18</sup>O, <sup>19</sup>F, <sup>23</sup>Na, <sup>27</sup>Al, <sup>28</sup>Si, <sup>29</sup>Si and <sup>30</sup>Si. The alpha-particle sub-library includes neutron production cross-sections, outgoing neutron energy and angular distribution data. JENDL is a truly evaluated library providing recommended nuclear data. Cross-sections in the JENDL library are typically derived from the measurements also included in EXFOR, with adjustments made to account for disagreements between different measurements and nuclear model codes (mainly using the mEXIFON [70] and EGNASH-2 [71] codes) used to aid the extrapolation of these data. In some cases, the total neutron production cross-section is adjusted to reproduce measured thick-target neutron yields. All data in ENDF-6 format can be retrieved from the dedicated page on the website of the JAEA Nuclear Data Center.

TENDL (TALYS-based Evaluated Nuclear Data Library) [68] is a major nuclear data library that provides the output of the TALYS nuclear model code system for direct use in both basic physics and applications. TENDL contains evaluations for seven types of incident particles (neutrons, protons, deuterons, tritons, <sup>3</sup>He,  $\alpha$ -particles, and  $\gamma$ -rays), for about 2800 isotopes and up to energies of 200 MeV for some cases. The 11<sup>th</sup> version is TENDL-2021, based on both default and adjusted TALYS calculations and data from other sources. First release was in 2008 and the latest ones are TENDL-2015, TENDL-2017, TENDL-2019 and TENDL-2021. Since 2015, TENDL is mainly developed at PSI and the IAEA (Nuclear Data Section). Data files are openly available<sup>7</sup>. In the alpha sub-library, tabulated data for total and partial cross-section data and spectra for virtually all

<sup>4</sup><http://www-nds.iaea.org/exfor>.

<sup>5</sup><http://www.nndc.bnl.gov/exfor>.

<sup>6</sup><https://wwwndc.jaea.go.jp/jendl/jendl.html>.

<sup>7</sup>[https://tendl.web.psi.ch/tendl\\_2021/talys.html](https://tendl.web.psi.ch/tendl_2021/talys.html).

isotopes can be found, including the  $(\alpha, xn)$  process; energy is given in MeV and cross-section in mb. Evaluated formatted data (ENDF) are also available. Both total non-elastic cross-section and cross-sections for explicit reaction channels are provided, although some problems are reported for the latter in [72] for several isotopes.

TABLE II: Isotopes for which  $(\alpha, n)$  cross-sections are catalogued in the EXFOR and JENDL databases.

Isotope	EXFOR	JENDL	Isotope	EXFOR	JENDL	Isotope	EXFOR	JENDL
<sup>6</sup> Li	Yes	Yes	<sup>7</sup> Li	Yes	Yes	<sup>8</sup> Li	Yes	No
<sup>9</sup> Be	Yes	Yes	<sup>10</sup> B	Yes	Yes	<sup>11</sup> B	Yes	Yes
<sup>12</sup> C	No	Yes	<sup>13</sup> C	Yes	Yes	<sup>14</sup> N	Yes	Yes
<sup>15</sup> N	Yes	Yes	<sup>16</sup> O	Yes	No	<sup>17</sup> O	Yes	Yes
<sup>18</sup> O	Yes	Yes	<sup>19</sup> F	Yes	Yes	<sup>20</sup> Ne	Yes	No
<sup>21</sup> Ne	Yes	No	<sup>22</sup> Ne	Yes	No	<sup>23</sup> Na	Yes	Yes
<sup>24</sup> Mg	Yes	No	<sup>25</sup> Mg	Yes	No	<sup>26</sup> Mg	Yes	No
<sup>27</sup> Al	Yes	Yes	<sup>28</sup> Si	Yes	Yes	<sup>29</sup> Si	Yes	Yes
<sup>30</sup> Si	Yes	Yes	<sup>31</sup> P	Yes	No	<sup>34</sup> S	Yes	No
<sup>35</sup> Cl	Yes	No	<sup>41</sup> K	Yes	No	<sup>40</sup> Ca	Yes	No
<sup>48</sup> Ca	Yes	No	<sup>45</sup> Sc	Yes	No	<sup>46</sup> Ti	Yes	No
<sup>48</sup> Ti	Yes	No	<sup>51</sup> V	Yes	No	<sup>50</sup> Cr	Yes	No
<sup>55</sup> Mn	Yes	No	<sup>54</sup> Fe	Yes	No	<sup>59</sup> Co	Yes	No
<sup>58</sup> Ni	Yes	No	<sup>60</sup> Ni	Yes	No	<sup>62</sup> Ni	Yes	No
<sup>64</sup> Ni	Yes	No	<sup>63</sup> Cu	Yes	No	<sup>65</sup> Cu	Yes	No
<sup>64</sup> Zn	Yes	No	<sup>66</sup> Zn	Yes	No	<sup>68</sup> Zn	Yes	No
<sup>70</sup> Zn	Yes	No	<sup>69</sup> Ga	Yes	No	<sup>71</sup> Ga	Yes	No
<sup>70</sup> Ge	Yes	No	<sup>72</sup> Ge	Yes	No	<sup>74</sup> Ge	Yes	No
<sup>76</sup> Ge	Yes	No	<sup>75</sup> As	Yes	No	<sup>76</sup> Se	Yes	No
<sup>86</sup> Sr	Yes	No	<sup>89</sup> Y	Yes	No	<sup>93</sup> Nb	Yes	No
<sup>92</sup> Mo	Yes	No	<sup>94</sup> Mo	Yes	No	<sup>100</sup> Mo	Yes	No
<sup>98</sup> Ru	Yes	No	<sup>107</sup> Ag	Yes	No	<sup>109</sup> Ag	Yes	No
<sup>115</sup> In	Yes	No	<sup>121</sup> Sb	Yes	No	<sup>123</sup> Sb	Yes	No
<sup>130</sup> Te	Yes	No	<sup>127</sup> I	Yes	No	<sup>181</sup> Ta	Yes	No

Isotopes for which there exist experimentally measured and evaluated cross-sections that overlap with the energy range of interest are summarized in Tab. II. While the available data cover most naturally occurring isotopes, several lack data, many of which may be important for low-background experiments. These isotopes are summarized in Tab. III. Elements for which the missing isotopes constitute an  $\mathcal{O}(1)$  contribution to the total neutron yield relative to the dominant contributor are colored red, as computed by NeuCBOT [73] for 10 MeV  $\alpha$ -particles, using cross-sections computed

TABLE III: Naturally occurring isotopes for which there are currently no measured  $(\alpha, n)$  cross-sections in the 4–10 MeV energy range cataloged in EXFOR. Elements for which \* is listed for the mass number have no data available for any of their naturally existing isotopes. In addition to the isotopes listed below, data are lacking for all elements with atomic numbers larger than that of Iodine, with the exception of  $^{131}\text{Ta}$ . Red elements (all except Ni and V) are those for which missing isotopes constitute an  $\mathcal{O}(1)$  contribution to the element’s total neutron yield at natural abundance, relative to the dominant contributor.

$^{32,33,36}\text{S}$	$^{37}\text{Cl}$	*Ar	$^{39,40}\text{K}$	$^{42-44,46}\text{Ca}$	$^{47,49,50}\text{Ti}$	$^{50}\text{V}$
$^{52-54}\text{Cr}$	$^{56-58}\text{Fe}$	$^{61}\text{Ni}$	$^{67}\text{Zn}$	$^{73}\text{Ge}$	$^{74,77,78,80,82}\text{Se}$	*Br
*Kr	*Rb	$^{84,87,88}\text{Sr}$	*Zr	$^{95,96-98}\text{Mo}$	$^{96,99-102,104}\text{Ru}$	*Rh
*Pd	*Cd	$^{113}\text{In}$	*Sn	$^{120,122-126,128}\text{Te}$		

by TALYS. In addition to the isotopes explicitly listed in this table, cross-section measurements do not exist for all other isotopes with atomic numbers greater than that of iodine, with the exception of  $^{181}\text{Ta}$ . However, we note that the total neutron yield of such heavy isotopes tends to be low: for example, NeuCBOT predicts an  $(\alpha, n)$  yield of  $7 \times 10^{-11}$  n/ $\alpha$  for natural xenon at 10 MeV.

Elements that are lacking  $(\alpha, n)$  cross-section measurements are typically in the mid- $Z$  range, including metals and noble gases, along with other elements that are commonly used in detector structural materials or as targets for low-background experiments.

A detailed comparison of the results from JENDL/AN-2005 and TENDL-2014, TENDL-2015, and TENDL-2017 is done in [72]; TENDL is found to provide larger neutron production cross-sections in most of the cases, with a few exceptions.

## B. Models

Depending on the kinetic energy  $E_\alpha$  of the incident  $\alpha$  particle, various reactions can occur<sup>8</sup>: below the Coulomb barrier of the target nucleus  $X$ , the incident particle may scatter elastically  $X(\alpha, \alpha)X$ , at higher energies, inelastic scattering  $X(\alpha, \alpha')X^*$  may leave the target nucleus  $X$  in an excited level. At low energies and especially for deformed nuclei this may be a collective excitation e.g. rotation or vibration. At higher energies, stripping reactions may cause a neutron emission. Above the Coulomb barrier, the incident  $\alpha$  can be captured: after a pre-equilibrium phase, the incident nucleons are thermalized, resulting in the creation of a compound nucleus  $^{A+2}_{Z+2}X^*$  excited by the added energy: both the kinetic energy of the  $\alpha$  and the binding energy  $S_\alpha$ . The compound nucleus may de-excite via several decay channels: e.g. either via  $\gamma$  transition to the ground state or, if the incident energy  $E_\alpha + S_\alpha$  is a multiple of the neutron separation energy  $S_n$ , via the emission of one or more neutrons together with one or more  $\gamma$  particles, i.e.  $(\alpha, n)$ ,  $(\alpha, n\gamma)$ ,  $(\alpha, 2n\gamma)$ ,  $(\alpha, 2n2\gamma)$ ,  $\dots$ ,  $(\alpha, xn\gamma)$  with the related exclusive excitation functions  $\sigma_{\alpha, xn\gamma}(E_\alpha)$ . Of interest for us is the excitation function for at least one neutron in the decay channel:  $\sigma_{\alpha, n}(E_\alpha) = \sum_x \sum_y \sigma_{\alpha, xn\gamma}(E_\alpha)$ .

<sup>8</sup>See e.g. [74] for an introduction into nuclear reaction theory.

In the range of resolved resonances on individual levels, i.e. where the width of the peaks in  $\sigma_{\alpha,n}(E_\alpha)$  is smaller than their spacing, the reaction has to be described by R-matrix theory (see e.g. [75]). Once the spacing drops below the peak's width in the range of unresolved resonances, the reaction can be treated in a statistical way. As the spacing depends on the level density that increases with the mass of the nucleus, the energy below which the statistical treatment breaks down increases with decreasing nuclide mass.

The formation and decay of the compound nucleus can be statistically treated by the Hauser-Feshbach theory [76]. Generally, the exit channels are treated as independent of the entrance channel; remaining correlations between them at low energy are treated by *width fluctuation corrections*. The transmission coefficients for the entrance and exit channels are commonly calculated within an optical model (see e.g. [77, 78]), i.e. describing the elastic scattering and the inelastic scattering via the real and imaginary parts of a complex optical model potential (OMP), respectively. The basic OMPs for spherical nuclides may be generalized for deformed nuclides to coupled-channels (CC) optical models. For weak coupling, the distorted wave-Born approximation (DWBA) can be applied to the CC OMP. Albeit by definition the statistical treatment cannot describe the resolved resonances, it can describe the average behaviour of the relevant physical quantities in this energy range [79]: based on these average values and the underlying distributions, it is possible to randomly sample resonances to populate the range of resolved resonances. Albeit the individual resonances created this way depend on the used random seeds, their average behaviour is physical sound.

Concerning the OMPs, they can be broadly divided in two classes [78]: phenomenological or microscopic OMPs. For both classes, models may include dispersion, i.e. do not treat the real and imaginary parts of the complex potential as independent, and hence reducing ambiguities in their parameters. The microscopic OMPs rely on folding the target matter distribution with OMP in nuclear matter, whereas phenomenological OMPs parameterize experimental data, either for an individual nuclide (*local* OMP) or for a larger set of nuclides (*global* OMP). Global phenomenological OMPs are optimized in such a way that, on average, they reproduce cross-sections close to the experimental ones for all non-actinide nuclides. This means there are some nuclides, for example,  $^{13}\text{C}$ , for which the calculated numbers are not very reliable, and extra tuning or even changing to a dedicated local OMP is desirable. For a discussion of suitable OMPs, see section VI A.

Nuclear reaction codes that implement the relevant models, and which are widely used and actively maintained, are TALYS and EMPIRE. Both use external tools for OMP calculations: TALYS relies on ECIS-06<sup>9</sup> [80]; also EMPIRE can use ECIS-06 but offer alternatively OPTMAN in the unpublished version 12<sup>10</sup> [81] which has an improved treatment of rotational levels for CC calculations. As both TALYS and EMPIRE are based on similar statistical models, their results are not significantly different from each other. A comprehensive comparison between the two codes, TALYS and EMPIRE, and experimental data for several key nuclides has been reported in Ref. [6, 82].

## V. NEUTRON YIELD CALCULATION TOOLS

The codes to calculate neutron yields and spectra require a number of inputs, such as the energy-dependent cross-sections of  $(\alpha, n)$  reactions, transition probabilities to excited states and stopping

<sup>9</sup>Available at <https://www-nds.iaea.org/RIPL-3/codes/ECIS/>.

<sup>10</sup>The older version 10 is available at <https://www-nds.iaea.org/RIPL-3/codes/OPTMAN/>.

power of  $\alpha$ -particles in different materials. These codes also need material composition where a particular reaction occurs,  $\alpha$ -energy or concentration of radioactive nuclei in the material.

Transition probabilities to excited states (sometimes called excitation functions) are usually known from calculations similar to those done for the cross-sections. Measurements are scarce and usually contain data from the first few excited states.

Alpha-particles produced in radioactive decay quickly lose energy in a material via ionisation and excitation of atoms, thus reducing the probability of neutron production. While energy loss of  $\alpha$ -particles is assumed to be well understood and is taken into account in all codes dealing with neutron yield calculation, uncertainties in models can sometimes be important. In particular, the breakdown of Bragg's law in composite low- $Z$  materials may result in uncertainties up to 50 % [83].

### A. Stopping power calculation

$\alpha$  particles can be produced by the naturally occurring radioactive decay induced by some actinides.  $^{238}\text{U}$ ,  $^{232}\text{Th}$  and  $^{235}\text{U}$  are present on the Earth's crust at the  $\approx$ ppm (particle per million) level and have decay chains in which several alpha decays are produced in series. Their initial energy is between 4–10 MeV, so the range of energies 0–10 MeV needs to be considered to account for the energy loss in the material before the interaction. Nowadays, there exist several codes and libraries for the calculation of the stopping power in various materials. For the specific case of the alpha projectile and the codes presented in this paper, the programs of reference are *ASTAR* (*SaG4n*) and *SRIM* (*SOURCES4A* and *NeuCBOT*).

The NIST *ASTAR* code [84] calculates the stopping power of alpha particles in 74 media based on the methods described in the ICRU 49 report [85]. The stopping power is given in the energy range from 1 keV to 1 GeV. Tables are differentiated for solid and gaseous targets as differences up to 10 % are expected [83]. In the high energy range ( $E_\alpha > 2$  MeV) the stopping power is calculated using Bethe's formulas and includes the shell, Barkas and Bloch, and the density-effect corrections, while in the low energy range models based on experimental data are used. When experimental data for the single elements are not available, values are interpolated among the existing ones [84]. In case of composite material without experimental data, the cumulative stopping power is calculated by linearly adding the stopping power of each element in the compound (Bragg's additivity law). The *SaG4n* code uses the stopping tables from *Geant4*, which are based on the ICRU 49 report in the low energy range ( $E < 8$  MeV) and the Bethe-Bloch formula in the high energy one.

The Stopping and Range of Ions in Matter (*SRIM*) code [86], on the other hand, uses a quantum mechanical treatment of projectile-target atoms collisions to calculate the stopping power and range of various ions (projectiles), including  $\alpha$ -particles, in matter (target atoms). In the case of compound materials, the code takes into account the energy loss due to the bonding electrons, correcting Bragg's additivity law. This is shown to be particularly important for low- $Z$  materials, such as hydrocarbons, where chemical bonding effects can result in up to 50 % deviations between data and calculations [83]. *SRIM* has the flexibility to manually input the target's compound based on its molecular weights in addition to the target material's list, which is included in the NIST database. Similar to the *ASTAR* database, *SRIM* allows the selection of a solid or gaseous target. For  $\alpha$ -particles the range is extended up to 8 GeV.

Several authors have performed comparisons between the *ASTAR* and *SRIM* calculations for a range of materials [87–90]. The two calculations are generally in good agreement, typically within

a few percent. When compared to data, the result is highly dependent on the material. The ASTAR (ICRU) program states an uncertainty of the order of 1–2% for single elements and 1–4% for compound materials for  $\alpha$ -particles in the energy range of interest for alphas from radioactivity (2–8 MeV). For lower energy  $\alpha$ -particles ( $E < 1$  MeV), the uncertainty increases with the decrease of the energy, reaching about 30% for 1 keV  $\alpha$ -particles [84]. SRIM’s authors report that, for  $\alpha$  ions, 89% of the calculations performed with the code agree within 10% with the experimental data [86].

## B. SOURCES4

The computer code SOURCES4 [91, 92] uses the libraries of  $\alpha$ -emission lines from radioactive isotopes, cross-sections of  $(\alpha, n)$  reactions either from calculations or experimental data, excitation functions (probabilities of transitions to excited states) and energy losses of  $\alpha$ -particles in different materials, to calculate the neutron production rate and energy spectra of emitted neutrons. The most recent version is SOURCES4C [92] but for historical reasons, the older version SOURCES4A [91] is used by some collaborations. The release notes from the authors and previous tests showed that, if the same cross-sections and branching ratios are used in both versions of the code, there is no difference between the results for almost all isotopes.

The code was modified to extend the  $\alpha$  energy range from 6.5 MeV (as in the original version) to about 10 MeV (see [93] for the modifications of the SOURCES4A code). More cross-sections and branching ratios calculated using the EMPIRE 2.19 [94], EMPIRE 3.2.3 and TALYS [65] codes were added to the library of SOURCES4 code covering the range of alpha energies up to 10 MeV [6, 93, 95–98]. A comparison of cross-sections from EMPIRE 2.19 with experimental data was published in Refs. [93, 98] and the results of neutron yield calculations with modified SOURCES4A were used for a number of dark matter experiments (see, for example, Refs. [99–102]). The accuracy of the calculation was estimated to be about 20% based on the comparison of neutron yields obtained with different sets of cross-sections [93].

The user input to SOURCES4A includes material composition (where an  $\alpha$  source is located), isotopic composition for each element (only isotopes with cross-sections present in the code library can be included) and either the energy of the  $\alpha$ -particle or the radioactive isotope (or several isotopes in the case of decay chains, for instance) with the number of atoms in a sample. For application in low-background experiments an option of the thick target neutron yield is used, meaning that the size of the sample is much bigger than the range of alphas and edge effects can be neglected.

The output of SOURCES4A includes several files that return the neutron yield and spectra for the sum of the ground and all excited states, as well as neutron spectra for individual states. In the case of decay chains, neutron production from individual radioactive isotopes on each isotope in the material sample is also calculated. SOURCES4A/SOURCES4C do not calculate  $\gamma$ -ray production but the total energy transferred to  $\gamma$ -rays can be calculated from the energy of the excited states.

Cross-sections from recent versions of the nuclear physics codes TALYS [65] and EMPIRE 3.2.3 [94] have become available over the past few years and were added to the SOURCES4A libraries. The comparison between early neutron yield calculations with cross-sections from EMPIRE 2.19, TALYS 1.9 and EMPIRE 3.2.3) has recently been published [6].

SOURCES4A libraries are regularly updated as described in Ref. [6]. Recent development in-

cludes optimisation of the cross-sections and branching ratios used in the calculations by selecting a combination of the experimental data and the most reliable model for a particular isotope [103]. For low- $Z$  materials, the measurements are used where available since none of the codes based on statistical models can reliably predict  $(\alpha, n)$  cross-sections. These data are complemented by the calculations from `EMPIRE` or `TALYS 1.9` to extend the cross-sections to higher energies and to obtain branching ratios usually unavailable from limited data sets. The optimisation is being validated by comparing the neutron yield as a function of  $\alpha$  energy with the available data.

### C. NeuCBOT

NeuCBOT (the Neutron Calculator Based On TALYS) allows the user to specify a material composition—either by element, assuming natural abundances, or by isotope—and a material contamination level. Material contamination can be described either with a list of  $\alpha$ -particle energies or  $\alpha$ -emitting isotopes, all weighted by their desired relative abundance. NeuCBOT then simulates  $\alpha$ -particles slowing down in the material and integrates over the  $(\alpha, n)$  cross-section and emitted neutron spectrum at each step.

Stopping powers are read from a library generated by `SRIM` and summed together assuming Bragg’s rule of addition. If the user specified contamination levels by the  $\alpha$ -emitting isotopes, a local database is built by retrieving `ENSDF` files from the NNDC NuDat database, and  $\alpha$  energies and branching ratios are retrieved. The  $(\alpha, n)$  cross-sections and emitted neutron spectra are drawn from a `TALYS`-generated database. This database can be generated locally if the user has a local version of `TALYS` installed, or it can be retrieved from a remote database, which is generated for all naturally occurring isotopes for  $\alpha$  energies up to 10 MeV. To reduce disk space used in the latter case, the databases are only retrieved for each needed element and stored locally. NeuCBOT-V1 uses a database generated with `TALYS 1.6`, while NeuCBOT-V2 uses `TALYS 1.95`. Generally, NeuCBOT-V1  $(\alpha, n)$  yields were found to agree with similar calculations uses `JENDL` to within about 30% in most cases, with a few cases where bigger disagreement is seen, and the yields calculated by NeuCBOT are typically higher. For NeuCBOT-V2, a significant decrease in yield is found, bringing the values into closer agreement with numerical integrals over `JENDL` data. A more recent version, NeuCBOT-V3 allows the user to select evaluated cross-sections from the `JENDL` library where available, rather than those simulated by `TALYS`. Additional upgrades are currently under development, including calculations of correlated  $\gamma$ -ray yields and correlations between outgoing neutron energy and energy lost by the  $\alpha$  particle prior to capture.

### D. SaG4n

Until recently, the general-purpose radiation transport simulation codes like `Geant4` [104] were not able to calculate  $(\alpha, n)$  yields with sufficient accuracy due to the difficulty of realistically modeling the low-energy  $\alpha$  reactions. Since version 10.2, released in 2015, `Geant4` has incorporated the so-called `ParticleHP` module [105], which is able to use data libraries originally written in `ENDF-6` format to manage the non-elastic nuclear reactions of low energy ( $<200$  MeV) charged particles. These data libraries contain information describing nuclear interactions, in particular reaction cross-sections and secondary particle production. This allows modeling of the  $(\alpha, n)$  reactions with much higher precision than was possible previously, based on theoretical models implemented in

the code.

SaG4n [72, 106] is a Geant4-based code specifically developed for the calculation of  $(\alpha, n)$  neutron yields. SaG4 code<sup>11</sup> works for Geant4.10.6 (or later versions).

Unlike other codes, SaG4n employs explicit transport of incident  $\alpha$  particles through the material and generates neutrons one by one as the nuclear reactions occur. Unlike other codes that use neutron production cross-sections and stopping power data tables, this approach enables the simulation of both the neutron production and the neutron transport with Geant4, providing detailed information about each individual  $(\alpha, n)$  reaction that is not available otherwise. This feature is crucial for accurately calculating background events produced by  $(\alpha, n)$  neutrons, especially in rare event search experiments. Although SaG4n requires a longer computation time than other codes, this issue is sufficiently mitigated by well-known biasing techniques that enhance the neutron production rate and reduce the overall computational load.

Additionally, SaG4n allows the simulation of much more complex geometries than other codes, improving significantly on the accuracy of the results relevant to the interfaces between different materials. This is particularly important, for example, for accurate modeling of the effect of the surface  $\alpha$ s from the Rn daughter plate-out on the material surfaces, thus, controlling this type of background and the related systematic uncertainty.

Finally, depending on the information present in the data library used, SaG4N is, in principle, able to generate neutrons and  $\gamma$ -rays in coincidence, as well as other secondary particles emitted in the same nuclear reaction (not available yet with the current version of libraries). This feature allows the tagging of neutron-induced nuclear recoils using gammas in dark matter direct detection experiments.

SaG4n is flexible in selecting the data libraries to be used and allows a user to implement the desired modifications to the input/output files. By default, JENDL data library is used. In the case that the nuclide is not present in this database, TENDL is used. The format of the code output is flexible, but, in its original version, the code includes the initial position and momentum of the generated  $\alpha$ , position and momentum of the produced neutron (and  $\gamma$  rays, if generated), and the ‘weight’ of the event. The latter was introduced to compensate for the biasing that was necessary to enhance the neutron production rate for  $(\alpha, n)$  reactions.

### E. Comparison between the codes

A detailed comparison between the codes is beyond the scope of this paper. Thick target neutron yields from beams of alpha particles and naturally occurring radioactive decay chains from several different codes in comparison with experimental data have been published in Refs. [6, 72, 73, 107–109]. Most codes are continuously developing and updated with new cross-sections so previous publications may not reflect the current status of the codes. We show here (Table IV) a comparison between the 3 codes described above in calculating neutron yields from U/Th decay chains for widely used elements in detector components of low-background experiments.

---

<sup>11</sup>Available at <http://win.ciemat.es/SaG4n>.

TABLE IV: Neutron yield from ( $\alpha, n$ ) reactions in the  $^{238}\text{U}$  and  $^{232}\text{Th}$  decay chains in several materials as calculated by different codes. (1.07% of  $^{13}\text{C}$  has been assumed for natural carbon.)

Material	Neutron yield, $\text{g}^{-1} \text{s}^{-1} \text{ppb}^{-1}$ , as calculated by		
	SOURCES4	NeuCBOT v-3.0 (JENDL)	SaG4n (JENDL)
Carbon, $^{238}\text{U}$	$1.71 \times 10^{-11}$	$1.24 \times 10^{-11}$	$1.18 \times 10^{-11}$
Carbon, $^{232}\text{Th}$	$7.04 \times 10^{-12}$	$5.21 \times 10^{-12}$	$5.10 \times 10^{-12}$
Fluorine, $^{238}\text{U}$	$1.34 \times 10^{-9}$	$1.00 \times 10^{-9}$	$1.21 \times 10^{-9}$
Fluorine, $^{232}\text{Th}$	$5.35 \times 10^{-10}$	$4.45 \times 10^{-10}$	$5.23 \times 10^{-10}$
Aluminium, $^{238}\text{U}$	$1.67 \times 10^{-10}$	$1.40 \times 10^{-10}$	$1.48 \times 10^{-10}$
Aluminium, $^{232}\text{Th}$	$8.25 \times 10^{-11}$	$7.57 \times 10^{-11}$	$8.02 \times 10^{-11}$

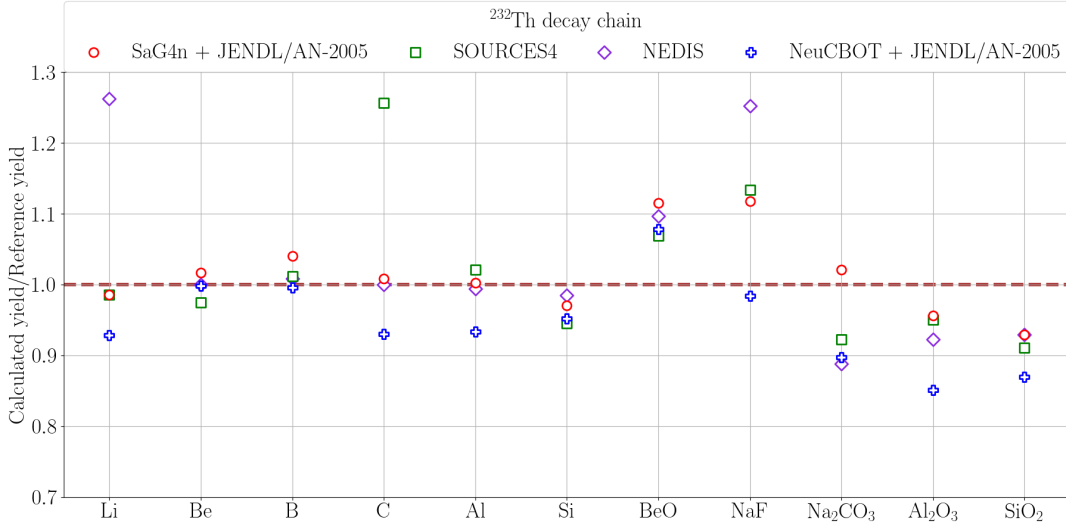


FIG. 6: Comparison of neutron yields calculated for light nuclei by applying different codes, including the upgraded version of NeuCBOT. The numerical values are normalized to evaluated data from various alpha-beam measurements [109] in order to demonstrate agreement between the calculations and measurements. The comparison in question is performed only for the thorium series.

## VI. TYPICAL UNCERTAINTIES IN NEUTRON YIELD CALCULATIONS

Predicting the neutron fluxes induced by ( $\alpha, n$ ) reactions in a material is a complex calculation, the uncertainty of which depends on multiple factors. In low background experiments, for instance, the neutron yield depends on factors such as the concentration of the radiogenic contaminants in the detector components, the chemical (actually isotopic) composition of the materials, and the

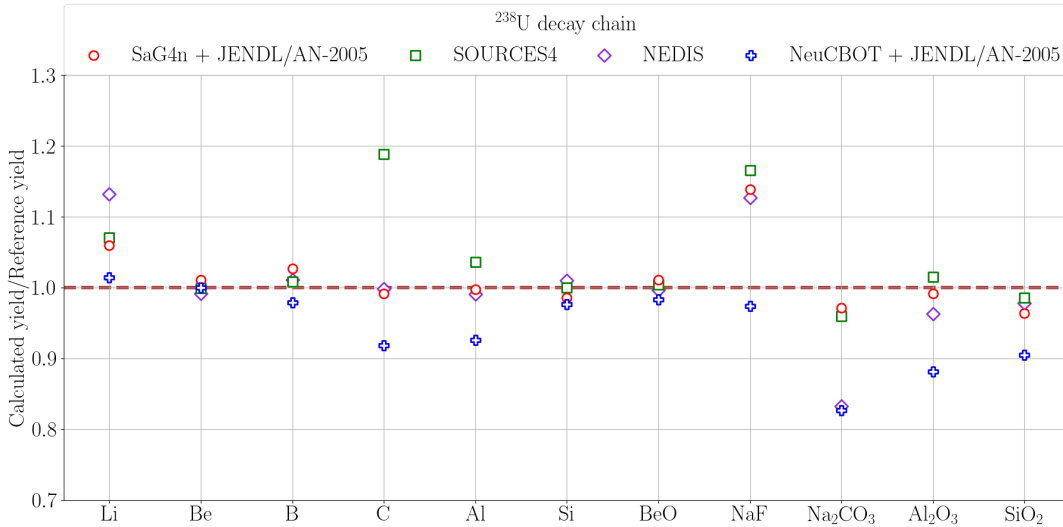


FIG. 7: Comparison of neutron yields calculated for light nuclei by applying different codes, including the upgraded version of NeuCBOT. The numerical values are normalized to evaluated data from various alpha-beam measurements [109] in order to demonstrate agreement between the calculations and measurements. The comparison in question is performed only for the uranium series.

uncertainty introduced by the calculation of alpha particle stopping power, as well as potential inaccuracies in cross-section data.

For common isotopes and materials relevant to rare event search experiments, the uncertainty in  $(\alpha, n)$  yield may fall within the range of 30%. In some other cases, it can reach much larger values, as high as  $\mathcal{O}(100\%)$ .

#### A. Cross sections: experimental data and nuclear model parameters

The low efficiency in detecting neutrons and the challenges associated with conducting neutron spectroscopy experiments justify the limited availability of energy-dependent experimental  $(\alpha, n)$  cross-section data in the EXFOR database for specific target isotopes, often lacking coverage across the entire energy range.

It is also possible that multiple measurements of the same isotope often disagree with each other, possibly due to differences in the experimental setups or the corrections applied when interpreting the results of the experiments. Furthermore, measurements catalogued by EXFOR often have inconsistent treatments of experimental uncertainties, often accounting for varying levels of precision.

For what concerns the evaluated cross section, the results of the nuclear reaction codes depend on the used models, the applied values for the model parameters, and even on the technical imple-

mentation of the models in code (e.g. on the binning of the level density tables [110]). Concerning the OMPs, the Reference Input Parameter Library for Calculation of Nuclear Reactions and Nuclear Data Evaluations (RIPL)<sup>12</sup> generally recommend in [78] to use local phenomenological when possible.

For  $(\alpha, n)$ -reactions, the chosen  $\alpha$ -OMP has the greatest impact on the obtained results [110]. RIPL list in [78] several global  $\alpha$ -OMP suitable for  $\alpha$ -induced reactions, see table V. Out of these, the model `Avrigeanu2014` [111] is the most recent<sup>13</sup>. In addition, an  $\alpha$ -OMP can be constructed from nucleon OMPs by `Watanabe`'s folding approach [113, 114].

From the newer global, phenomenological nucleon-nucleus OMP contained in RIPL-3 [78], only two, `KoningDelaroche2003` [115] and `Morillon2006` [116, 117], covers partial our nuclide and energy ranges of interest. The latter is a dispersive model and also of `KoningDelaroche2003` exists an unpublished dispersive version, which is provided by TALYS 1.96 [66]. It provides also local OMPs covering some of our nuclides of interest [115]; further local OMP are listed in [78] and [118, Annex 5.D]. With the JLM model of `Bauge et al.` [119] exists also a microscopic OMP that partially covers the relevant nuclides. Both TALYS and EMPIRE can read OMPs from RIPL; in addition TALYS provides the models `Avrigeanu2014` [111, 120] and `Demetriou2002` [121, table 1] which are not part of RIPL-3 and finally the possibility to read in tabulated OMPs from a user-provided file.

Further properties that affect the results are nuclear mass, nuclear structure, level density, and photon strength function; whereas the impact of the width fluctuation correction is only minor [110]. An overview of available models is given e.g. in RIPL [78]. For several combinations of target nuclides and projectiles, the TENDL library provides also "best" settings and error estimations for these properties, which can be used in TALYS [66, 68]. In the current TALYS version, "best" settings are mostly available for incident neutrons and gammas and not for alphas; in this case, TALYS falls back to its default settings and their uncertainties.

Table V summarize the relevant models and data sets for the calculation of the  $(\alpha, n)$  -excitation function. Uncertainties on the calculation are caused by the propagation of the uncertainties on the model parameter whereas the selection of a particular, inaccurate model may cause a systematic uncertainty. One has also to note that for the ten lightest nuclides in table II calculations with TALYS or EMPIRE are not suitable because the nuclide masses are below the applicability range of any of the listed OMPs. At this mass range, R-matrix theory may be a more suitable approach than the statistical treatment.

With TALYS, together with the auxiliary tool `TASMAN`<sup>14</sup>, it is possible to randomly sample the parameter space of the input parameters within the parameter's uncertainties and hence propagate these uncertainties to the result of TALYS [68]<sup>15</sup>, i.e. in our case the excitation function of  $(\alpha, n)$  reactions, see fig. 8 for an example.

---

<sup>12</sup>Available at <https://www-nds.iaea.org/RIPL-3/>.

<sup>13</sup>Note that the different model `Avrigeanu1994` [112] is only suitable for  $\alpha$  emission, see [78].

<sup>14</sup>`TASMAN` is not public, but can be obtained from the TALYS authors upon request.

<sup>15</sup>Within the TALYS-related literature, this approach is called *Total Monte Carlo*. [68].

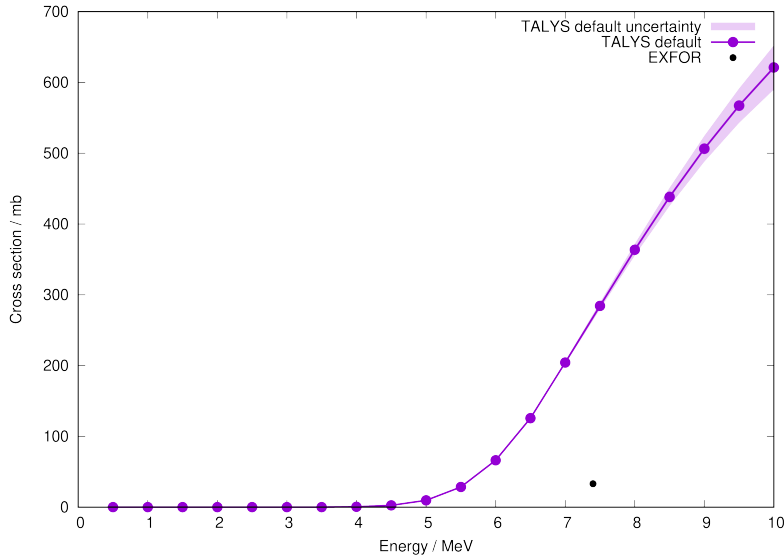


FIG. 8: Excitation function for  $^{40}\text{Ar}(\alpha, n)$  (dark violet line) as calculated with TALYS 1.96 based on default settings, see also table V. The associated uncertainty (light violet band) is based on sampling the input parameter space with TASMANT: 2750 samples within the parameter’s uncertainties were drawn. For comparison, the only existing measurement by Schwartz *et al.* [122] from the EXFOR data base is shown (black data point). (Figure created by H. Kluck for this publication.)

TABLE V: Nuclear models relevant for calculating the  $(\alpha, n)$  excitation function; a “p” indicates a phenomenological model, a “m” indicates a microscopic model. A hollow bullet ( $\circ$ ) in the second and third column indicates if they are available in TALYS or EMPIRE, a filled bullet ( $\bullet$ ) indicate the default option, a square ( $\square$ ) indicate the model can be loaded from the RIPL database, if the official manuals give no information a question mark is set.

Model or data set	Type	Available in ...		Comments
		TALYS 1.96	EMPIRE 3.2	
Global $\alpha$ -OMP				
Avrigeanu2014	p	$\bullet$		[111, 120], $45 \leq A \leq 209$ , $E \lesssim 12$ MeV
Kumar2006	p		$\bullet$	[123], $12 \leq A \leq 209$ , $E < 140$ MeV

Continued on next page

TABLE V: Nuclear models relevant for calculating the  $(\alpha, n)$  excitation function; a “p” indicates a phenomenological model, a “m” indicates a microscopic model. A hollow bullet ( $\circ$ ) in the second and third column indicates if they are available in TALYS or EMPIRE, a filled bullet ( $\bullet$ ) indicate the default option, a square ( $\square$ ) indicate the model can be loaded from the RIPL database, if the official manuals give no information a question mark is set. (Continued)

Model or data set	Type	Available in ...		Comments
		TALYS 1.96	EMPIRE 3.2	
KoningDelaroche2003	p	$\circ$		[66, 115], folding approach, $24 \leq A \leq 209$ , $2 \text{ keV} \leq E \leq 200 \text{ MeV}$
Demetriou2002-1	p	$\circ$		[121, table 1], $E \lesssim 12 \text{ MeV}$
Demetriou2002-1	p	$\circ$		[121, table 2], $E \lesssim 12 \text{ MeV}$
Demetriou2002-dis	p	$\circ$		[121], $E \lesssim 12 \text{ MeV}$ , dispersive model
Strohmaier1982	p	$\square$	$\square$	[124], $40 \leq A \leq 100$ , $1 \text{ MeV} \leq E \leq 30 \text{ MeV}$
McFadden1966	p	$\circ$	$\square$	[125], $16 \leq A \leq 208$ , $1 \text{ MeV} \leq E \leq 25 \text{ MeV}$
Huizenga1962	p	$\square$	$\square$	[126], $20 \leq A \leq 235$ , $1 \text{ MeV} \leq E \leq 46 \text{ MeV}$
<b>Global nucleon-OMP</b>				
Morillon2004	p	$\square$	$\square$	[116, 117], dispersive model, $27 \leq A \leq 209$ , $1 \text{ keV} \leq E \leq 200 \text{ MeV}$
KoningDelaroche2003	p	$\bullet$	$\square$	[115], $24 \leq A \leq 209$ , $1 \text{ keV} \leq E \leq 200 \text{ MeV}$
KoningDelaroche2003-dis	p	$\circ$		[66, 115], dispersive model, $24 \leq A \leq 209$ , $1 \text{ keV} \leq E \leq 200 \text{ MeV}$
JLM-MOM	m	$\circ$		[119] Jeukenne-Lejeune-Mahaux calculation with MOM code, $40 \leq A \leq 209$ , $E \leq 200 \text{ MeV}$
<b>Nuclear mass</b>				
AME2020	p	$\bullet$		[127], the Atomic Mass Evaluation

Continued on next page

TABLE V: Nuclear models relevant for calculating the  $(\alpha, n)$  excitation function; a “p” indicates a phenomenological model, a “m” indicates a microscopic model. A hollow bullet ( $\circ$ ) in the second and third column indicates if they are available in TALYS or EMPIRE, a filled bullet ( $\bullet$ ) indicate the default option, a square ( $\square$ ) indicate the model can be loaded from the RIPL database, if the official manuals give no information a question mark is set. (Continued)

Model or data set	Type	Available in ...		Comments
		TALYS 1.96	EMPIRE 3.2	
Goriely2016	m	$\circ$		[128], Gogny-Hartree-Fock-Bogoliubov nuclear mass model
FRDM	m	$\circ$		[129], Finite-Range Droplet Macroscopic model
Goriely2009	m	$\circ$		[130], Skyrme-Hartree-Fock-Bogoliubov nuclear mass model
DZ	m	$\circ$		Duflo-Zuker mass formula, unpublished
Nuclear structure			?	
RIPL3		$\circ$		[78], only experimental data
RIPL3+theo		$\bullet$		[66, 78], experimental data with theoretical extension
Theo		$\circ$		[66], only theoretical calculation
Level density				
EGSM	p		$\bullet$	[131], Enhanced Generalized Superfluid Model
GSM	p	$\circ$		[132], Generalized Superfluid Model
GSM-col	p	$\circ$	$\circ$	GSM including collective enhancement, TALYS and EMPIRE differ in the used parameters
BFM	p	$\circ$		[133–135], Back-shifted Fermi gas Model
BFM-col	p	$\circ$		BFM including collective enhancement

Continued on next page

TABLE V: Nuclear models relevant for calculating the  $(\alpha, n)$  excitation function; a “p” indicates a phenomenological model, a “m” indicates a microscopic model. A hollow bullet ( $\circ$ ) in the second and third column indicates if they are available in TALYS or EMPIRE, a filled bullet ( $\bullet$ ) indicate the default option, a square ( $\square$ ) indicate the model can be loaded from the RIPL database, if the official manuals give no information a question mark is set. (Continued)

Model or data set	Type	Available in . . .		Comments
		TALYS 1.96	EMPIRE 3.2	
CTM	p	$\bullet$	$\circ$	[136], Constant Temperature Model, TALYS and EMPIRE differ in the used parameterization
CTM-col	p	$\circ$		CTM including collective enhancement
Hilaire2012	m	$\circ$		[137], temperature-dependent Gogny-Hartree-Fock-Bogoliubov model
Goriely2008	m	$\circ$	$\circ$	[138], deformed Skyrme-Hartree-Fock-Bogoliubov model
Goriely2001	m	$\circ$		[139], Hartree-Fock model
<b>Photon strength function</b>				
MLO3	p		$\circ$	[140], Modified Lorentzian model
MLO2	p		$\circ$	[140], Modified Lorentzian model
MLO1	p		$\bullet$	[140], Modified Lorentzian model
GFL	p		$\circ$	[141], Generalized Fermi Liquid model
EGLO	p	$\circ$	$\circ$	[142, 143], Enhanced Generalized Lorentzian model
SLO	p	$\bullet$	$\circ$	[144, 145], Standard Lorentzian model
HFB-QRPA-D1M	m	$\circ$		[146], D1M Gogny-Hartree-Fock-Bogoliubov model
Daoutidis2012	m	$\circ$		[147], temperature-dependent relativistic mean field model

Continued on next page

TABLE V: Nuclear models relevant for calculating the  $(\alpha, n)$  excitation function; a “p” indicates a phenomenological model, a “m” indicates a microscopic model. A hollow bullet ( $\circ$ ) in the second and third column indicates if they are available in TALYS or EMPIRE, a filled bullet ( $\bullet$ ) indicate the default option, a square ( $\square$ ) indicate the model can be loaded from the RIPL database, if the official manuals give no information a question mark is set. (Continued)

Model or data set	Type	Available in . . .		Comments
		TALYS 1.96	EMPIRE 3.2	
HFBCS-QRPA-Tdep	m	$\circ$		[148], temperature-dependent Skyrme-Hartree-Fock- Bogoliubov model
HFBCS-QRPA	m	$\circ$		[148], Skyrme-Hartree-Fock- Bogoliubov model
HFBCS	m	$\circ$		[149], Skyrme-Hartree-Fock BCS model
Goriely1998		$\circ$		[150], hybride model
Width fluctuation correction				
GOE		$\circ$		[151], Gaussian Orthogonal Ensemble of Hamiltonian matrices-model
HRTW		$\circ$	$\bullet$	[152], Hofmann-Richert- Tepel-Weidenmüller model
Moldauer1980			$\bullet$	[153]

## B. Assay results

The source of the neutrons generated in the  $(\alpha, n)$  reactions are alpha emitters coming mostly from the U-chain. The activity concentrations must be measured for all relevant materials and specific isotopes, or at least for sub-chains, which are in equilibrium - see the discussion in Sec. III A and Fig. 1. The activities in the upper part of the U-chain, assayed with the help of mass spectrometry (ICP-MS), are determined with a precision of about 10–40 %. It is assumed here that the measurements are performed with the highest sensitivities (sub 0.1 ppt  $\simeq 1 \mu\text{Bq kg}^{-1}$ ). ICP-MS may be also used to investigate the high-purity material contamination not only with radioactive isotopes, but also with various elements down to  $10^{-9}$  g/g [154]. The typical uncertainty of such measurements is about 30 %. This may be interesting especially if elements with high cross section for  $(\alpha, n)$  reactions are considered. ICP-MS may also be applied to determine the isotopic composition (stable and long-lived isotopes) of the material in question. Depending on the isotopes, the precision of its abundance determination may vary from 1–30 % [154].

Measurements of  $^{226}\text{Ra}$ ,  $^{222}\text{Rn}$  and its short-lived daughters (down to  $^{214}\text{Po}$ , middle part of the U-chain, see Fig. 1) close to the detection limits ( $\approx 10 \mu\text{Bq kg}^{-1}$ ) are also performed with a typical

precision of about 30 % [25].

The lower part of the U-chain ( $^{210}\text{Pb}$ – $^{210}\text{Po}$ ) is assayed with the lowest sensitivity of about  $1 \text{ mBq kg}^{-1}$ . The procedure requires extensive chemistry to separate  $^{210}\text{Po}$  from the sample matrix, deposit it on a dedicated disc, and count the activity. A time series of  $^{210}\text{Po}$  measurements allows to determine the  $^{210}\text{Pb}$  activity concentration with the precision of about 15–20 % [155].

To conclude, one can state that the measurements of the activity concentrations of alpha emitters are performed with a precision of about 30 %. One should underline here that this concerns tests performed with the highest available sensitivities and applying various techniques (mass spectrometry, gamma counting, chemical separation of  $^{210}\text{Po}$ ). If lower sensitivities are required the precision is higher, in average 15–20 % depending on the sample and technique.

### C. Material composition

In the assessment of potential neutron backgrounds for next-generation rare event search detectors, the uncertainty regarding the chemical composition of the materials is frequently overlooked. Typically, detector construction material assays primarily concentrate on measuring the radioactivity levels of Uranium and Thorium chains. Nevertheless, as introduced in Section III A, the material composition should always be investigated in detail and assayed if necessary, to incorporate it as an input for Monte Carlo simulations of  $(\alpha, n)$  process.

The uncertainty on neutron production due to  $(\alpha, n)$  having its origin in the elemental composition of a given material has several factors to include. The first factor is the basic information on the uncertainty with which the elemental composition of a given material is known. In the best case, the information is known with the certified information from the producer. If not, the elemental analysis of the material of interest could be done with some known precision, usually on a 15–20 % level. To speed up the assay process for groups of similar materials, "educated guess" technique can be applied introducing even less accountable uncertainty.

Another noteworthy factor is the uniformity of the material under consideration. The key question is to what extent the MC simulation can define the geometric structure in detail. A perfect example of non-homogeneous and troublesome but necessary materials are the electronic parts. For example, common resistors where the changes in placement of layers of borosilicate glass within the small simulated volume give visible effects in the neutron yield simulation.

The statistical analysis of the simulated data (SaG4n code) for assayed materials was performed and it confirmed that there are chemical elements of special interest. Those elements make a great contribution to neutron production due to their large cross-section on  $(\alpha, n)$  process. Example of such chemical elements are: Aluminum, Fluorine, or Boron. Their presence in a very small fraction inside the material, contributes on the level of several percent to the neutron production quota. Therefore the variation in mass fraction within the material of such element significantly contributes to the total neutron yield uncertainty. This shows that the propagation of uncertainty on the mass fraction of the element into the neutron yield calculation is not straightforward and should be done with care. As an example, the study done for the resistor used for the light readout system is presented in Table VI. The chemical elements are listed based on their contribution to neutron yield, and the nominal mass fraction value provides the most accurate information for simulating

the input material.

TABLE VI: The chemical composition of a resistor is given with the element’s mass fraction as assumed in the MC simulation model and calculated expected neutron yield due to  $(\alpha, n)$  reactions. The neutron production is calculated based on the SaG4n simulation and measured radioactivity level of Uranium and Thorium chains.

Element	Nominal mass fraction	Neutron yield / $\text{kg}^{-1} \text{s}^{-1}$
Al	0.33	$3.21 \times 10^{-5}$
B	0.01	$8.30 \times 10^{-6}$
O	0.55	$3.07 \times 10^{-6}$
Mg	0.01	$7.06 \times 10^{-7}$
Si	0.04	$3.82 \times 10^{-7}$
Ca	0.01	$7.53 \times 10^{-9}$
Ni	0.02	$1.11 \times 10^{-9}$
Cu	0.01	$5.52 \times 10^{-10}$

## VII. DATA NEEDS

The success of the accurate  $(\alpha, n)$  neutron yield calculation for spent fuel management, low-background experiments, and nuclear astrophysics heavily relies on accurate experimental data and nuclear models. Unfortunately, much of the existing experimental data is outdated, incomplete, and characterized by significant or inconsistent uncertainties in the cross-sections. Furthermore, experimental data on neutron emission angular distributions are rare, and information regarding partial cross-sections and correlated  $\gamma$ -ray emission is even more scarce. Consequently, the evaluated nuclear libraries suffer from incompleteness (i.e. only a few isotopes are available) or reliance on outdated evaluations. Calculations involving numerous isotopes require combining evaluated cross-section files, relying on experimental data, with theory-driven cross-section files or nuclear models.

Recognizing the urgency to update nuclear data libraries for charged-particle-induced reactions, and  $(\alpha, n)$  in particular, the IAEA’s Nuclear Data Section (NDS) has initiated a global collaborative effort [156]. This initiative aims to produce updated and reliable data for charged-particle-induced reactions. Notably,  $\text{UF}_6$  and  $\text{PuF}_4$  fuel, discrepancies between new evaluations and the 1991 reference data reached the 25-50 % level, emphasizing the critical need for accurate  $^{19}\text{F}(\alpha, n)$  reaction cross-sections.

New massive argon-based detectors for the search of rare events have been proposed or are in the construction phase [1, 157]. For these experiments, the direct measurement of the  $(\alpha, n)$  cross-section on  $^{40}\text{Ar}$  is crucial for accurate background calculations, as experimental data for this element are either very old or essentially absent in the large part of the energy range of interest.

The imperative for enhanced experimental and evaluated data libraries extends beyond the  $^{19}\text{F}$  and the  $^{40}\text{Ar}$  cases, encompassing  $(\alpha, n)$  reactions across various light and medium-light elements

essential for diverse applications. The data available in the EXFOR database show large inconsistencies with respect to the reported uncertainties, and  $(\alpha, xn)$  and  $(\alpha, n\gamma)$  cross-sections data are particularly limited. Furthermore, the development of nuclear reaction codes, particularly those employing R-matrix and statistical models, as well as source codes used for calculating neutron sources from existing cross-section and stopping-power data, necessitates continuous updates.

To adequately address these demands for new measurements, improved data libraries, and sophisticated software, an international collaboration is paramount. Coordinated efforts among interdisciplinary groups actively involved in  $(\alpha, n)$  studies can substantially enhance our comprehension of this reaction and match the nuclear data needs in different fields of science and applications.

#### ACKNOWLEDGMENTS

The CIEMAT group is funded by the Spanish Ministry of Science (MICINN) through the grant PID2022-138357NB-C22 and the project PID2021-123100NB-I00 funded by MCINN/AEI/1013039/501100011033/FEDER, UE. This work was also funded in the framework of the NCN Opus research grant (UMO2019/33/B/ST2/02884). V.K. is supported by the STFC (grant ST/W000547/1) and the University of Sheffield. S.W. is sponsored by the University of California, Riverside (USA). M.P. and I.L. acknowledge financial support from the contract no. 04/2022, Programme 5, Module 5.2 CERN-RO. A.K. is supported by the Fermi Research Alliance, LLC under Contract No. DE-AC02-07CH11359 with the U.S. Department of Energy, Office of Science, Office of High Energy Physics. V.L. is supported by the Fundação para a Ciência e a Tecnologia FCT-Portugal (grant 2021.01039.CEECIND). M.G. acknowledges the Russian grant No. 075-15-2024-541.

- 
- [1] C. E. Aalseth *et al.* (DarkSide-20k), *Eur. Phys. J. Plus* **133**, 131 (2018).
  - [2] A. H. Abdelhameed *et al.* (CRESST), *Phys. Rev. D* **100**, 102002 (2019).
  - [3] J. Aalbers *et al.* (LZ), *Phys. Rev. Lett.* **131**, 041002 (2023).
  - [4] E. Aprile *et al.* (XENON), *Phys. Rev. Lett.* **131**, 041003 (2023).
  - [5] J. Cooley *et al.*, *Nucl. Instrum. Methods Phys. Res. A* **888**, 110 (2018).
  - [6] V. A. Kudryavtsev, P. Zakhary, and B. Easeman, *Nucl. Instrum. Methods Phys. Res. A* **972**, 164095 (2020).
  - [7] M. T. Pigni, S. Croft, and I. C. Gauld, *Prog. Nucl. Energy* **91**, 147 (2016).
  - [8] R. Acciarri *et al.* (DUNE), *Long-Baseline Neutrino Facility (LBNF) and Deep Underground Neutrino Experiment (DUNE): Conceptual Design Report, Volume 1: The LBNF and DUNE Projects*, Tech. Rep. (Fermilab,, 2016) [arXiv:1601.05471](https://arxiv.org/abs/1601.05471) [physics.ins-det].
  - [9] J. B. Albert *et al.* (nEXO), *Phys. Rev. C* **97**, 065503 (2018).
  - [10] A. Abusleme *et al.* (JUNO), *JHEP* **11** (102).
  - [11] A. Allega *et al.* (SNO+), *Phys. Rev. Lett* **130**, 091801 (2023).
  - [12] W. Wilson, R. Perry, W. Charlton, and T. Parish, *Progress in Nuclear Energy* **51**, 608 (2009).
  - [13] T. Martínez *et al.*, *Nucl. Data Sheets* **120**, 78 (2014).
  - [14] B. E. Watt, *Phys. Rev.* **87**, 1037 (1952).
  - [15] G. Zuzel, M. Wojcik, C. Buck, W. Rau, and G. Heusser, *Nucl. Instrum. Meth. A* **498**, 240 (2003).
  - [16] D. Leonard *et al.*, *Nucl. Instrum. Meth. Phys. Res. A* **591**, 490 (2008).
  - [17] S. Cebrián *et al.*, *Journal of Instrumentation* **10** (05), P05006.
  - [18] N. Abgrall *et al.*, *Nucl. Instrum. Meth. Phys. Res. A* **828**, 22 (2016).

- [19] D. Leonard *et al.*, *Nucl. Instrum. Meth. Phys. Res. A* **871**, 169 (2017).
- [20] S. Cebrián *et al.*, *Journal of Instrumentation* **12** (08), T08003.
- [21] E. Aprile *et al.*, *Eur. Phys. J. C* **77**, 890 (2017).
- [22] D. Akerib *et al.*, *Eur. Phys. J. C* **80**, 1044 (2020).
- [23] M. Agostini *et al.*, *Eur. Phys. J. C* **78**, 388 (2018).
- [24] B. LaFerriere, T. Maiti, I. Arnquist, and E. Hoppe, *Nucl. Instrum. Meth. A* **775**, 93 (2015).
- [25] H. Nesser, G. Heusser, and L. Laubenstein, *Appl. Rad. Isot* **53**, 191 (2000).
- [26] G. Zuzel, private communication (2023).
- [27] G. Zuzel, M. Wojcik, and H. Simgen, *Int. J. Mod. Phys. A* **32**, 1743004 (2017).
- [28] G. Zuzel and M. Wojcik, *Nucl. Instrum. Meth. A* **676**, 140–148 (2012).
- [29] G. Zuzel, K. Pelczar, and M. Wojcik, *Appl. Rad. Isot.* **126**, 165 (2017).
- [30] M. Wojcik, W. Wlazlo, G. Zuzel, and G. Heusser, *Nucl. Instrum. Meth. A* **449**, 158–171 (2000).
- [31] M. Zykova *et al.*, *Materials* **14**, 3757 (2021).
- [32] E. Mozhevitina *et al.*, *AIP Conf. Proc.* **1672**, 050001 (2015).
- [33] A. Chepurinov, S. Nisi, M. L. d. Vacri, and Y. Suvorov, *AIP Conf. Proc.* **1549**, 161 (2013).
- [34] W. Bothe and W. Gentner, *Zeitschrift für Physik* **112**, 45 (1939).
- [35] E. M. Burbidge, G. R. Burbidge, W. A. Fowler, and F. Hoyle, *Rev. Mod. Phys.* **29**, 547 (1957).
- [36] K. S. Krane, *Introductory nuclear physics* (Wiley, New York, NY, 1988).
- [37] P. Descouvemont, *Front. Astron. Space Sci.* **7**, 9 (2020).
- [38] L. Dardelet *et al.*, in *XIII Nuclei in the Cosmos (NIC XIII)* (2014) p. 145.
- [39] M. Hampel, R. J. Stancliffe, M. Lugaro, and B. S. Meyer, *The Astrophysical Journal* **831**, 171 (2016).
- [40] M. Hampel, A. I. Karakas, R. J. Stancliffe, B. S. Meyer, and M. Lugaro, *The Astrophysical Journal* **887**, 11 (2019).
- [41] R. B. Walton, J. D. Clement, and F. Boreli, *Phys. Rev.* **107**, 1065 (1957).
- [42] K. K. Sekharan, A. S. Divatia, M. K. Mehta, S. S. Kerekatte, and K. B. Nambiar, *Phys. Rev.* **156**, 1187 (1967).
- [43] C. N. Davids, *Nuclear Physics A* **110**, 619 (1968).
- [44] J. K. Bair and F. X. Haas, *Phys. Rev. C* **7**, 1356 (1973).
- [45] H. W. Drotleff *et al.*, *Astrophys. J.* **414**, 735 (1993).
- [46] S. E. Kellogg, R. B. Vogelaar, and R. W. Kavanagh, *Bull. Am. phys. Soc.* **34**, 1192 (1989).
- [47] S. Harissopulos *et al.*, *Phys. Rev. C* **72**, 062801 (2005).
- [48] P. S. Prusachenko *et al.*, *Phys. Rev. C* **105**, 024612 (2022).
- [49] B. Gao *et al.* (JUNA Collaboration), *Phys. Rev. Lett.* **129**, 132701 (2022).
- [50] G. G. Kiss *et al.*, *The Astrophysical Journal* **908**, 202 (2021).
- [51] T. N. Szegedi *et al.*, *Phys. Rev. C* **104**, 035804 (2021).
- [52] Angus, Cameron *et al.*, *EPJ Web Conf.* **279**, 11003 (2023).
- [53] A. Favalli, S. Croft, R. Venkataraman, and M. Pigni, INMM Proceedings - 59th INMM Annual Meeting (2019).
- [54] P. J. Mohr, *The European Physical Journal A* **51**, 1 (2015).
- [55] S. M. Qaim, I. Spahn, B. Scholten, and B. Neumaier, *Radiochimica Acta* **104**, 601 (2016).
- [56] Breunig, Katharina *et al.*, *EPJ Web Conf.* **146**, 08006 (2017).
- [57] M. J. Welch and K. D. McElvany, *Radiochimica Acta* **34**, 41 (1983).
- [58] F. Guérard, J.-F. Gustin, and M. W. Brechbiel, *Cancer Biotherapy and Radiopharmaceuticals* **28**, 1 (2013), PMID: 23075373.
- [59] P. Albertsson *et al.*, *Frontiers in Medicine* **9**, 1076210 (2023).
- [60] R. H. Larsen, B. W. Wieland, and M. R. Zalutsky, *Applied Radiation and Isotopes* **47**, 135 (1996).
- [61] F. Ditrói *et al.*, *Nucl. Instrum. Methods Phys. Res. B* **436**, 119 (2018).
- [62] C. Tsopelas and H. Hendrikse, *The Scientific World Journal* **2015**, 676719 (2015).
- [63] M. Herman *et al.*, *Nuclear Data Sheets* **108**, 2655 (2007).
- [64] M. Herman *et al.*, *EMPIRE-3.2 Malta (rev.1)*, techreport INDC(NDS)-0603 (International Nuclear Data Committee (INDC), 2015).
- [65] A. J. Koning and D. Rochman, *Nucl. Data Sheets Special Issue on Nuclear Reaction Data*, **113**, 2841 (2012).

- [66] S. G. Arjan Koning, Stephane Hilaire, *TALYS-1.96/2.0* (2021).
- [67] O. Iwamoto *et al.*, *Journal of Nuclear Science and Technology* **60**, 1 (2023).
- [68] A. J. Koning *et al.*, *Nucl. Data Sheets Special Issue on Nuclear Reaction Data*, **155**, 1 (2019).
- [69] N. Otuka *et al.*, *Nucl. Data Sheets* **120**, 272 (2014).
- [70] T. Murata, *Modification of exifon code and analysis of  $\alpha + n$  reactions in  $E_n = 20\text{--}50$  meV* (1997).
- [71] N. Yamamuro, *A nuclear cross section calculation system with simplified input-format* (1990).
- [72] E. Mendoza *et al.*, *Nucl. Instrum. Meth. A* **960**, 163659 (2020).
- [73] M. B. Gromov, S. Westerdale, I. A. Goncharenko, and A. S. Chepurinov, *Physics of Atomic Nuclei* **86**, 181 (2023).
- [74] C. A. Bertulani and P. Danielewicz, *Introduction to Nuclear Reactions* (CRC Press, 2019).
- [75] P. Descouvemont and D. Baye, *Reports on Progress in Physics* **73**, 036301 (2010).
- [76] W. Hauser and H. Feshbach, *Physical Review* **87**, 366 (1952).
- [77] B. V. Carlson, in *Workshop on nuclear reaction data and nuclear reactors: Physics, design and safety*, edited by N. Paver, M. Herman, and A. Gandini (2001).
- [78] R. Capote *et al.*, *Nuclear Data Sheets* **110**, 3107 (2009).
- [79] D. Rochman, A. Koning, J. Kopecky, J.-C. Sublet, P. Ribon, and M. Moxon, *Annals of Nuclear Energy* **51**, 60 (2013).
- [80] J. Raynal, in *Computing as a Language of Physics: Lectures Presented at an International Seminar Course at Trieste from 2 to 20 August 1971 Organized by the International Centre for Theoretical Physics, Trieste*, edited by A. Salam (International Atomic Energy Agency, 1972) pp. 281–322.
- [81] E. S. Soukhovitskil *et al.*, *Supplement to OPTMAN Code, Manual Version 10 (2008)*, techreport JAERI - Data/Code 2008-025 (Japan Atomic Energy Research Institute, 2008).
- [82] P. Zakhary, *Neutron production in  $(\alpha, n)$  reactions*, MSc Dissertation, University of Sheffield (2019).
- [83] D. I. Thwaites, *Radiat. Res.* **95**, 495 (1983), publisher: Radiation Research Society.
- [84] *ASTAR, stopping-power and range tables for helium ions*, NIST, Physical Meas. Laboratory (2017).
- [85] *International Commission on Radiation Units and Measurements, ICRU Report 49, Stopping Powers and Ranges for Protons and Alpha Particles* (1993).
- [86] J. F. Ziegler, *SRIM - the stopping and range of ions in matters* (2013).
- [87] S. Kumar and P. K. Diwan, *Radiation Effects and Defects in Solids* **173:11-12**, 970 (2018).
- [88] M. Jassim and H. Tawfeek, *Advances in Physics Theories and Applications* **66**, 13 (2017).
- [89] M. Pigni, S. Croft, and I. Gauld, *Progress in Nuclear Energy* **91**, 147 (2016).
- [90] N. Hansson, C. Ekberg, and K. Spahiu, *Nuclear Materials and Energy* **22**, 100734 (2020).
- [91] W. B. Wilson *et al.*, *SOURCES4A: A Code for Calculating  $(\alpha, n)$ , Spontaneous Fission, and Delayed Neutron Sources and Spectra*, Tech. Rep. LA-13639-MS (Los Alamos National Laboratory, 1999).
- [92] W. B. Wilson, R. T. Perry, W. S. Charlton, T. A. Parish, and E. F. Shores, *Radiat. Prot. Dosim.* **115**, 117 (2005).
- [93] V. Tomasello, V. A. Kudryavtsev, and M. Robinson, *Nucl. Instrum. Meth. A* **595**, 431 (2008).
- [94] M. Herman *et al.*, *Nucl. Data Sheets Special Issue on Evaluations of Neutron Cross Sections*, **108**, 2655 (2007).
- [95] M. J. Carson *et al.*, *Astropart. Phys.* **21**, 667 (2004).
- [96] R. Lemrani, M. Robinson, V. A. Kudryavtsev, M. De Jesus, G. Gerbier, and N. J. C. Spooner, *Nucl. Instrum. Meth. A* **560**, 454 (2006).
- [97] V. Tomasello, M. Robinson, and V. A. Kudryavtsev, *Astropart. Phys.* **34**, 70 (2010).
- [98] V. Tomasello, *Background Simulations for a Large-scale Cryogenic Dark Matter Experiment*, PhD Thesis, University of Sheffield (2009).
- [99] G. Angloher *et al.* (EURECA), *Phys. Dark Univ.* **3**, 41 (2014).
- [100] E. Armengaud *et al.* (EDELWEISS), *Astropart. Phys.* **47**, 1 (2013).
- [101] D. S. Akerib *et al.* (LUX-ZEPLIN), *Phys. Rev. D* **101**, 052002 (2020).
- [102] E. Aprile *et al.* (XENON), *Phys. Rev. D* **100**, 052014 (2019).
- [103] V. A. Kudryavtsev, P. Krawczun, and R. Bocheva, *Neutron yield calculation from  $(\alpha, n)$  reactions with SOURCES4* (2022), proc. 8th Topical Workshop on Low Radioactivity Techniques (June 2022); arXiv:2211.02080.
- [104] S. Agostinelli *et al.* (GEANT4), *Nucl. Instrum. Meth. A* **506**, 250 (2003).

- [105] J. Allison *et al.*, *Nucl. Instrum. Meth. A* **835**, 186 (2016).
- [106] V. Pseudo *et al.*, *J. Phys. Conf. Ser.* **1468**, 012059 (2020).
- [107] S. Westerdale and P. D. Meyers, *Nucl. Instrum. Methods Phys. Res. A* **875**, 57 (2017).
- [108] G. N. Vlaskin, Y. S. Khomyakov, and V. I. Bulanenko, *At. Energy* **117**, 357 (2015).
- [109] A. C. Fernandes, A. Kling, and G. N. Vlaskin, *EPJ Web Conf.* **153**, 07021 (2017).
- [110] J. Pereira and F. Montes, *Phys. Rev. C* **93**, 034611 (2016).
- [111] V. Avrigeanu, M. Avrigeanu, and C. Mănăilescu, *Phys. Rev. C* **90**, 044612 (2014).
- [112] V. Avrigeanu, P. E. Hodgson, and M. Avrigeanu, *Physical Review C* **49**, 2136 (1994).
- [113] S. Watanabe, *Nuclear Physics* **8**, 484 (1958).
- [114] D. G. Madland, in *Proceedings of a Specialists Meeting on Preequilibrium Nuclear Reactions Semmering*, NEA/NEANDC(1988)245/U, edited by B. Strohmaier (OECD Publishing, 1988) pp. 103–110.
- [115] A. Koning and J. Delaroche, *Nuclear Physics A* **713**, 231 (2003).
- [116] B. Morillon and P. Romain, *Phys. Rev. C* **70**, 014601 (2004).
- [117] B. Morillon and P. Romain, *Phys. Rev. C* **74**, 014601 (2006).
- [118] International Atomic Energy Agency, *Handbook for Calculations of Nuclear Reaction Data, RIPL-2*, TEC-DOC Series No. 1506 (International Atomic Energy Agency, 2006).
- [119] E. Bauge, J. P. Delaroche, and M. Girod, *Phys. Rev. C* **63**, 024607 (2001).
- [120] M. Avrigeanu, A. Obreja, F. Roman, V. Avrigeanu, and W. von Oertzen, *Atomic Data and Nuclear Data Tables* **95**, 501 (2009).
- [121] P. Demetriou, C. Grama, and S. Goriely, *Nuclear Physics A* **707**, 253 (2002).
- [122] R. B. Schwartz, J. W. Corbett, and W. W. Watson, *Phys. Rev.* **101**, 1370 (1956).
- [123] A. Kumar, S. Kailas, S. Rathi, and K. Mahata, *Nuclear Physics A* **776**, 105 (2006).
- [124] B. Strohmaier, M. Uhl, and W. Reiter, *Neutron Cross Section Calculations for  $^{52}\text{Cr}$ ,  $^{55}\text{Mn}$ ,  $^{56}\text{Fe}$  and  $^{58,60}\text{Ni}$  for Incident Energies up to 30 MeV*, Tech. Rep. INDC(NDS)-128/GR (International Atomic Energy Agency: Nuclear Data Section, 1982).
- [125] L. McFadden and G. Satchler, *Nuclear Physics* **84**, 177 (1966).
- [126] J. Huizenga and G. Igo, *Nuclear Physics* **29**, 462 (1962).
- [127] W. Huang *et al.*, *Chinese Physics C* **41**, 030002 (2017).
- [128] S. Goriely, S. Hilaire, M. Girod, and S. Péru, *Eur. Phys. J. A* **52**, 202 (2016).
- [129] P. Möller, A. Sierk, T. Ichikawa, and H. Sagawa, *Atomic Data and Nuclear Data Tables* **109-110**, 1 (2016).
- [130] S. Goriely, N. Chamel, and J. M. Pearson, *Phys. Rev. Lett.* **102**, 152503 (2009).
- [131] A. D'Arrigo, G. Giardina, M. Herman, A. V. Ignatyuk, and A. Taccone, *Journal of Physics G: Nuclear and Particle Physics* **20**, 365 (1994).
- [132] A. V. Ignatyuk, J. L. Weil, S. Raman, and S. Kahane, *Physical Review C* **47**, 1504 (1993).
- [133] W. Dilg, W. Schantl, H. Vonach, and M. Uhl, *Nuclear Physics A* **217**, 269 (1973).
- [134] M. Grossjean and H. Feldmeier, *Nuclear Physics A* **444**, 113 (1985).
- [135] P. Demetriou and S. Goriely, *Nuclear Physics A* **695**, 95 (2001).
- [136] A. Gilbert and A. G. W. Cameron, *Canadian Journal of Physics* **43**, 1446 (1965).
- [137] S. Hilaire, M. Girod, S. Goriely, and A. J. Koning, *Phys. Rev. C* **86**, 064317 (2012).
- [138] S. Goriely, S. Hilaire, and A. J. Koning, *Physical Review C* **78**, 10.1103/physrevc.78.064307 (2008).
- [139] S. Goriely, F. Tondeur, and J. M. Pearson, *Atomic Data and Nuclear Data Tables* **77**, 311 (2001).
- [140] V. A. Plujko, S. N. Ezhov, M. O. Kavatsyuk, A. A. Grebenyuk, and R. V. Yermolenko, in *Proceedings, International Conference on Nuclear Data for Science and Technology (ND 2001): Embracing the Future at the Beginning of the 21st Century*, Vol. 39 (2002) pp. 811–814.
- [141] S. Mughabghab and C. Dunford, *Physics Letters B* **487**, 155 (2000).
- [142] J. Kopecky and M. Uhl, *Physical Review C* **41**, 1941 (1990).
- [143] J. Kopecky, M. Uhl, and R. E. Chrien, *Physical Review C* **47**, 312 (1993).
- [144] D. Brink, *Nuclear Physics* **4**, 215 (1957).
- [145] P. Axel, *Physical Review* **126**, 671 (1962).
- [146] S. Goriely, S. Hilaire, S. Péru, and K. Sieja, *Phys. Rev. C* **98**, 014327 (2018).
- [147] I. Daoutidis and S. Goriely, *Phys. Rev. C* **86**, 034328 (2012).
- [148] S. Goriely, E. Khan, and M. Samyn, *Nuclear Physics A* **739**, 331 (2004).

- [149] S. Goriely and E. Khan, *Nuclear Physics A* **706**, 217 (2002).
- [150] S. Goriely, *Physics Letters B* **436**, 10 (1998).
- [151] J. Verbaarschot, H. Weidenmüller, and M. Zirnbauer, *Physics Reports* **129**, 367 (1985).
- [152] H. M. Hofmann, T. Mertelmeier, M. Herman, and J. W. Tepel, *Zeitschrift für Physik A Atoms and Nuclei* **297**, 153 (1980).
- [153] P. Moldauer, *Nuclear Physics A* **344**, 185 (1980).
- [154] F. Marchegiani, F. Ferella, and S. Nisi, *MDPI Physics* **3**, 71 (2021).
- [155] T. Mroz, P. Czudak, G. Zuzel, and M. Wojcik, Studies of bulk  $^{210}\text{Po}/^{210}\text{Pb}$  contamination in high purity copper for low background detectors (2021), Talk at the TAUP Conference, Underground Laboratories Discussion Panel, 2021-09-03.
- [156] IAEA, (alpha,n) nuclear data evaluations and data needs. summary report of the technical meeting (2021).
- [157] P. Agnes *et al.* (Global Argon Dark Matter), *Phys. Rev. D* **107**, 112006 (2023).